

Systematic approach to leptogenesis in nonequilibrium QFT: vertex contribution to the CP -violating parameter

M. Garny^{a,b,*}, A. Hohenegger^{a,†}, A. Kartavtsev^{a,‡} and M. Lindner^{a,§}

^aMax-Planck-Institut für Kernphysik, Saupfercheckweg 1, 69117 Heidelberg, Germany

^bTechnische Universität München, James-Frank-Straße, 85748 Garching, Germany

The generation of a baryon asymmetry via leptogenesis is usually studied by means of classical kinetic equations whose applicability to processes in the hot and expanding early universe is questionable. The approximations implied by the state-of-the-art description can be tested in a first-principle approach based on nonequilibrium field theory techniques. Here, we apply the Schwinger–Keldysh/Kadanoff–Baym formalism to a simple toy model of leptogenesis. We find that, within the toy model, medium effects increase the vertex contribution to the CP -violating parameter. At high temperatures it is a few times larger than in vacuum and asymptotically reaches the vacuum value as the temperature decreases. Contrary to the results obtained earlier in the framework of thermal field theory, the corrections are only linear in the particle number densities. An important feature of the Kadanoff–Baym formalism is that it is free of the double-counting problem, i.e. no need for real intermediate state subtraction arises. In particular, this means that the structure of the equations automatically ensures that the asymmetry vanishes in equilibrium. These results give a first glimpse into a number of new and interesting effects that can be studied in the framework of nonequilibrium field theory.

PACS numbers: 11.10.Wx, 98.80.Cq

Keywords: Kadanoff–Baym equations, Boltzmann equation, expanding universe, leptogenesis

I. INTRODUCTION

The almost complete absence of antimatter on Earth, in the solar system and in hadronic cosmic rays suggests that the universe is baryonically asymmetric. This conclusion is confirmed by experimental data on the abundances of the light elements [1] and precise measurements of the cosmic microwave background spectrum [2, 3].

The baryon asymmetry of the universe can be generated dynamically provided the three Sakharov conditions [4] are fulfilled in the early universe: violation of baryon (or baryon minus lepton) number; violation of C and CP ; and deviation from thermal equilibrium. In the standard model supplemented by heavy right-handed Majorana neutrinos, these conditions are naturally satisfied for leptons. The Majorana mass term violates lepton number by two units. Complex Yukawa couplings of the right-handed neutrinos to leptons and the Higgs doublet induce CP violation. The rapid expansion of the universe causes a deviation from thermal equilibrium. Finally, the generated lepton asymmetry is converted to the observed baryon asymmetry by sphalerons [5, 6]. In other words the generation of the baryon asymmetry – baryogenesis – proceeds via the generation of a lepton asymmetry – leptogenesis [7].

Many aspects of leptogenesis have been extensively investigated. In particular, it has been shown that the

CP -violating parameter and the efficiency of leptogenesis are affected by the flavor structure of the neutrino Yukawa couplings [8–16]. In [17, 18] it was demonstrated that the CP -violating parameter is resonantly enhanced if two of the heavy neutrinos have mass differences comparable to their decay widths. Medium effects have also been addressed. In the hot and dense plasma the deviation of the CP -violating parameter and the thermal masses from their vacuum values plays an important role [19, 20]. In state-of-the-art calculations Boltzmann equations are used to compute the asymmetry. Their applicability in the hot and expanding early universe can be checked using a first-principle approach like the Schwinger–Keldysh/Kadanoff–Baym formalism. Some aspects of leptogenesis have been investigated within this framework at different levels of approximation in *Minkowski* space [21–25]. These studies were motivated by the expectation that in the expanding universe filled with hot and dense plasma quantum effects, which are neglected in the canonical treatment, might play a crucial role.

In this paper we investigate leptogenesis, and in particular the vertex contribution to the CP -violating parameter within the framework of nonequilibrium quantum field theory. Using the Kadanoff–Baym formalism as the starting point of our analysis, we derive *quantum-corrected Boltzmann equations*. We explicitly take medium corrections to the CP -violating parameter as well as the expanding background into account. The Kadanoff–Baym approach to the analysis of nonequilibrium systems is technically considerably more involved than the canonical Boltzmann ansatz. For this reason, before applying it to realistic models of leptogenesis, here we study a simple toy model containing one complex and

* mathias.garny@ph.tum.de

† andreas.hohenegger@mpi-hd.mpg.de

‡ alexander.kartavtsev@mpi-hd.mpg.de

§ manfred.lindner@mpi-hd.mpg.de

two real scalar fields. It is defined by the Lagrangian

$$\mathcal{L} = \frac{1}{2} \partial^\mu \psi_i \partial_\mu \psi_i - \frac{1}{2} M_i^2 \psi_i \psi_i + \partial^\mu \bar{b} \partial_\mu b - m^2 \bar{b} b - \frac{\lambda}{2!} (\bar{b} b)^2 - \frac{g_i}{2!} \psi_i b b - \frac{g_i^*}{2!} \psi_i \bar{b} \bar{b} + \mathcal{L}_{rest}, i = 1, 2, \quad (1)$$

where \bar{b} denotes the complex conjugate of b . Despite its simplicity, the model incorporates all features relevant for leptogenesis. The real scalar fields imitate the (two lightest) heavy right-handed neutrinos, whereas the complex scalar field models the baryons. The $U(1)$ symmetry, which we use to define “baryon” number, is explicitly broken by the presence of the last two terms, just as the $B - L$ symmetry is explicitly broken by Majorana mass terms in phenomenological models. Thus the first Sakharov condition is fulfilled. The couplings g_i model the complex Yukawa couplings of the right-handed neutrinos to leptons and the Higgs. By rephasing the complex scalar field at least one of the couplings g_i can be made real. If $\arg(g_1) \neq \arg(g_2)$ the other one remains complex and there is CP violation, as is required by the second Sakharov condition. In vacuum the vertex contribution to the CP -violating parameter is given by

$$\epsilon_i^{vac} = -\frac{1}{8\pi} \frac{|g_j|^2}{M_i^2} \text{Im} \left(\frac{g_i g_j^*}{g_i^* g_j} \right) \ln \left(1 + \frac{M_i^2}{M_j^2} \right), \quad (2)$$

see Appendix A. Just as in realistic models, the required deviation from thermal equilibrium is caused by the rapid expansion of the universe. Thus the third Sakharov condition is fulfilled as well. Finally, the quartic self-interaction term in (1) plays the role of the Yukawa and gauge interactions in established models – it brings the “baryons” to equilibrium. The renormalizability of the theory requires the presence of some additional terms, which are accounted for by \mathcal{L}_{rest} . By appropriately choosing the corresponding coupling constants we can always make the contributions of these terms negligibly small. Since the physically interesting range for the generation of the asymmetry is $0.1 M_i \lesssim T \lesssim 10 M_i$, where M_i is the mass of the lightest heavy particle, the running effects cannot make these couplings large during the relevant period.

Apart from the vertex contribution [7] to the CP -violating parameter discussed above, there is also a self-energy contribution [26–28]. In the Kadanoff–Baym formalism the analysis of the former is rather independent from the analysis of the latter. For this reason, in this paper, we consider only the vertex contribution, whereas the self-energy contribution will be addressed in [29]. To make the discussion more transparent we give the technical details in the appendices, whereas in the main body of the paper we discuss qualitative features of the employed approach and present the results.

- (i) As we argue in Sec. II, the formalism is free of the double-counting problem typical for the canonical Boltzmann approach. In other words the structure of the equations automatically ensures that

the asymmetry vanishes in thermal equilibrium and no need for the real intermediate state subtraction arises.

- (ii) Our result for the vertex contribution to the CP -violating parameter, presented in Sec. III, differs from that obtained in the framework of equilibrium thermal field theory by replacing the zero-temperature propagators with finite temperature propagators in the matrix elements of the Boltzmann equation [19, 20] – the medium corrections are only *linear* in the particle number densities. For scalars the medium effects always increase the CP -violating parameter, which in turn leads to an enhancement of the generated asymmetry.
- (iii) By comparing the CP -violating parameters obtained by using the Maxwell–Boltzmann (MB) and Bose–Einstein (BE) statistics, we find that quantum statistical effects play a considerable role. As we argue in Sec. III, the medium effects increase the CP -violating parameter by a factor of at most two in the Maxwell–Boltzmann approximation. At high temperatures, the increase is up to an order of magnitude larger when Bose enhancement is taken into account.

In Sec. IV we present numerical solutions of the quantum-corrected Boltzmann equations, and discuss the quantitative impact of medium effects on the final asymmetry within the toy model. Finally, in Sec. V, we summarize our results and present our conclusions.

II. NONEQUILIBRIUM DYNAMICS

To calculate the asymmetry generated at the epoch of leptogenesis one usually employs generalized Boltzmann equations for the one-particle distribution functions of the different particle species [1]:

$$p^\alpha \mathcal{D}_\alpha f_\psi(X, p) = \frac{1}{2} \int d\Pi_a^3 d\Pi_b^3 \dots d\Pi_i^3 d\Pi_j^3 \dots \times (2\pi)^4 \delta(p + p_a + p_b \dots - p_i - p_j) \times [|M_{i+j+\dots \rightarrow \psi+a+b\dots}^2 f_i f_j \dots (1 \pm f_a)(1 \pm f_b)(1 \pm f_\psi) - |M_{\psi+a+b\dots \rightarrow i+j+\dots}^2 f_a f_b f_\psi \dots (1 \pm f_i)(1 \pm f_j) \dots]. \quad (3)$$

The fourth line in Eq. (3) describes the decrease in number of species ψ due to the scattering (or decay) process $\psi + a + b \dots \rightarrow i + j + \dots$ and is usually referred to as the loss term. The third line describes the increase in the number of ψ due to the process $i + j + \dots \rightarrow \psi + a + b \dots$ and is referred to as the gain term. The Dirac δ function in the second line enforces energy-momentum conservation in each individual process, whereas the invariant phase-space elements $d\Pi^3$ ensure that the resulting expression is a Lorentz scalar. The probabilities of the decay and scattering processes are usually calculated in *vacuum*, which is inconsistent with the nonzero particle number densities. Moreover the canonical approach is plagued with

the *double-counting* problem. For instance, in the canonical approach, the scattering process $\ell h \rightarrow \tilde{\psi}_i \rightarrow \ell \bar{h}$ is equivalent to the inverse decay $(\ell h, \ell \bar{h} \rightarrow \psi_i)$ of the heavy Majorana neutrino followed by the decay $(\psi_i \rightarrow \ell h, \ell \bar{h})$ if the intermediate heavy neutrino $\tilde{\psi}_i$ is on-shell. That is, the same contribution is counted twice. As a consequence, a nonzero asymmetry is generated even in thermal equilibrium. The problem is accounted for by the *real intermediate state* subtraction procedure. Since the scattering amplitude is calculated in *vacuum*, one cannot assign a distribution function to the heavy neutrino $\tilde{\psi}_i$. For this reason the resulting collision terms are difficult to interpret. Only by assuming Maxwell-Boltzmann statistics and by integrating the resulting Boltzmann equations can one derive rate equations that manifestly lead to zero asymmetry in equilibrium.¹

Boltzmann equations rely on the concept of on-shell particles with constant mass. The spectral function $G_\rho(X, p)$ of a particle whose mass does not change as it propagates along a geodesic is orthogonal to its four-momentum [30]:

$$p^\alpha \mathcal{D}_\alpha G_\rho(X, p) = 0. \quad (4)$$

For a pointlike on-shell particle the spectral function is zero off-shell and diverges on-shell:

$$G_\rho(X, p) = 2\pi \text{sign}(p_0) \delta(p^\alpha p_\alpha - M^2). \quad (5)$$

Instead of using one-particle distribution functions, as the quantities describing the statistical properties of the system, we can use the statistical propagator $G_F(X, p)$:

$$G_F(X, p) \equiv [f_\psi(X, p) + \tfrac{1}{2}] G_\rho(X, p). \quad (6)$$

Written in terms of $G_\rho(X, p)$ and $G_F(X, p)$, a Boltzmann equation takes the form

$$p^\alpha \mathcal{D}_\alpha G_F(X, p) = \tfrac{1}{2} [\Pi_<(X, p) G_>(X, p) - G_<(X, p) \Pi_>(X, p)], \quad (7)$$

where $G_\gtrless \equiv G_F \pm \tfrac{1}{2} G_\rho$. Comparing Eqs. (7) and (3) we see that the quantities Π_\gtrless correspond to the loss and gain terms.

The transformations made so far simply seem to amount to a change of notation. However, the situation changes when one realizes that Eqs. (4) and (7) coincide with the equations that can be derived in a certain approximation from the system of Kadanoff-Baym equations and that the quantities Π_\gtrless can be identified with the self-energies. Despite the close similarity there

is an important difference: the self-energies calculated in the framework of the Kadanoff-Baym formalism differ from the gain and loss terms obtained in the canonical approach. As we will show in the following, the self-energies consistently take medium effects into account and the resulting equations are free of the double-counting problem.

The Kadanoff-Baym formalism may be viewed as *top-down* approach: starting from the complete evolution equations for the two-point functions, it is possible to derive kinetic equations in a systematic way by applying a number of well-known approximations [31–34]. We will refer to these equations as *quantum-corrected Boltzmann equations*. Within the Kadanoff-Baym formalism, both the overall structure of the equations as well as the scattering and decay rates are derived self-consistently from a common starting point based on the *in-in* or Schwinger-Keldysh description of nonequilibrium quantum fields. In contrast to that, within the canonical *bottom-up* approach, the scattering and decay rates are extracted from the S-matrix (i.e. based on the *in-out* formalism), and are then inserted into Boltzmann equations. We expect that both approaches are equivalent in the zero-temperature/zero-density and small coupling limit, where the mean-free path is large compared to the microscopic interaction length scales. In this regime, it may be considered that the top-down approach discussed here adds support to the usual bottom-up formalism. Additionally, as mentioned above, the top-down approach is free of the double-counting problem and allows one to explore the medium effects within nonequilibrium quantum field theory. This is especially relevant for the *CP*-violating terms, since these contain loop diagrams.

A. Kadanoff-Baym equations

The system of Kadanoff-Baym equations for the spectral function and the statistical propagator is usually formulated in coordinate space. For the complex scalar field b , which corresponds to baryons in our model they read (see Appendix B)

$$[\Box_x + m^2(x)] D_F(x, y) = \int_0^{y^0} \mathcal{D}^4 z \Sigma_F(x, z) D_\rho(z, y) - \int_0^{x^0} \mathcal{D}^4 z \Sigma_\rho(x, z) D_F(z, y), \quad (8a)$$

$$[\Box_x + m^2(x)] D_\rho(x, y) = \int_0^{y^0} \mathcal{D}^4 z \Sigma_\rho(x, z) D_\rho(z, y). \quad (8b)$$

As is clear from the terminology, the spectral function D_ρ contains information about spectral properties of the system, whereas the statistical propagator D_F contains information about its state. The spectral and statistical self-energies, Σ_ρ and Σ_F , as well as the effective mass $m^2(x) = m^2 + \Sigma_{loc}(x)$, which contains the local self-energy, carry information about the interactions in the

¹ Strictly speaking, the system (3) is incorrect in general if it involves unstable particles, because the matrix elements, computed in perturbation theory, do not necessarily meet the requirements for transition amplitudes in systems of Boltzmann equations. In cases such as the present (leptogenesis) subtle modifications (RIS subtraction) are necessary to obtain consistent results.

system. They describe scattering and mean-field effects, respectively. The invariant volume element,

$$\mathcal{D}^4 z \equiv \sqrt{-g} d^4 z, \quad g \equiv \det g_{\mu\nu},$$

ensures that the Kadanoff–Baym equations (8) can be applied to the analysis of out-of-equilibrium dynamics not only in Minkowski, but also in a general curved space-time. Particularly interesting for our purpose is the case of the expanding early universe [35].

Let us list some of the qualitatively important features. First of all, Eqs. (8) are written in terms of *re-summed* propagators, i.e. they take into account the full series of *daisy* and *ladder* diagrams (see e.g. [36]). Second, the characteristic *memory* integrals on the right-hand side integrate over the full time history of the evolution. In other words the Kadanoff–Baym equations are non-Markovian, i.e. are not local in time. It is very important that the Kadanoff–Baym equations do not rely on the concept of quasiparticles and their collisions in the plasma. In other words, they are free of any possible uncertainties associated with definition of quasiparticle excitations in the hot plasma of the rapidly expanding universe. This property makes the Kadanoff–Baym equations a prime candidate for the analysis of leptogenesis. If the quasiparticle picture is applicable, they account for the time-dependence of the quasiparticle parameters. In particular, an effective time-dependent mass and width induced by the interactions of the system can be extracted from the Wigner-transform of the spectral function [37]. Finally, for weakly coupled systems close to thermal equilibrium the Kadanoff–Baym equations can be reduced to the Boltzmann equation [31–34], which we have briefly discussed above.

The Kadanoff–Baym equations for a system of n real scalar fields read [29, 30]

$$[\square_x + M_i^2] G_F^{ij}(x, y) = \int_0^{y^0} \mathcal{D}^4 z \Pi_F^{ik}(x, z) G_F^{kj}(z, y) - \int_0^{x^0} \mathcal{D}^4 z \Pi_\rho^{ik}(x, z) G_F^{kj}(z, y), \quad (9a)$$

$$[\square_x + M_i^2] G_\rho^{ij}(x, y) = \int_{x^0}^{y^0} \mathcal{D}^4 z \Pi_\rho^{ik}(x, z) G_\rho^{kj}(z, y), \quad (9b)$$

where the propagators and self-energies are now n -by- n matrices. The off-diagonal components of the propagators and self-energies describe the mixing of the fields.

Equations (8) and (9) are valid for a system of one complex and n real scalar fields with arbitrary interactions. Here, we consider $n = 2$. The information about the particular form of the interactions is encoded in the corresponding self-energies $\Sigma(x, y)$ and $\Pi^{ij}(x, y)$. The latter ones can be derived by functional differentiation of the two-particle-irreducible (2PI) effective action, $\Gamma_2[G, D]$, with respect to the two-point correlation functions $D(y, x)$ and $G^{ji}(y, x)$, see [30] and Appendix B for more details. The effective action is given by the sum of

all 2PI diagrams with vertices as given by the interaction Lagrangian and internal lines representing the complete connected two-point functions [38]. Of course the number of 2PI diagrams contributing to the effective action is infinite in any theory and the infinite sum must be truncated in a suitable way. To obtain a qualitative similarity between the toy model and the established models, we must take into account processes which generate and washout the asymmetry. The minimal set of relevant 2PI contributions is presented in Fig. 1. Clearly, after cutting

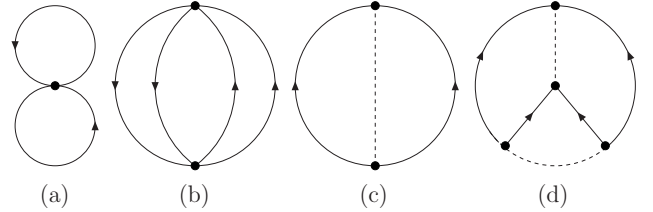


FIG. 1: Relevant two- and three-loop contributions to the 2PI effective action.

any two lines of the diagrams (a) – (d) they still remain connected. To understand which physical processes are described by the above diagrams in the Boltzmann approximation one has to discriminate between local and nonlocal contributions. The local diagram (a) generates

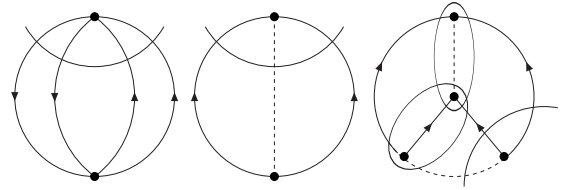


FIG. 2: Processes described by the 2PI diagrams in Fig. 1.

the mean-field correction $\Sigma^{\text{loc}}(x)$ to the effective mass $m^2(x)$ of the field:

$$\Sigma^{\text{loc}}(x) = \lambda D(x, x). \quad (10)$$

The nonlocal diagrams (b)–(d) describe scattering and decay processes, which can be identified by cutting the diagrams into two pieces by drawing a connected line in all possible ways as indicated in Fig. 2 (see also [39]). Cutting diagram (b), we obtain squares of tree-level amplitudes of $bb \rightarrow bb$ and $b\bar{b} \rightarrow b\bar{b}$ scattering processes. Analogously, cutting diagram (c), we get squares of the tree-level amplitudes of $\psi_i \rightarrow bb$ and $\psi_i \rightarrow b\bar{b}$ decay processes. In the canonical approach the decays of the heavy real scalars are CP -conserving at tree-level. To leading order the vertex CP -violating parameter ϵ is generated by interference of the tree-level and one-loop vertex decay amplitudes. In the Kadanoff–Baym formalism the leading vertex CP -violating contribution is described by

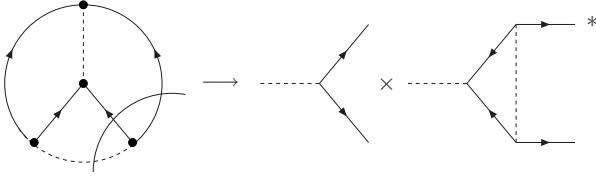


FIG. 3: Interference of the tree-level and one-loop vertex decay amplitudes.

diagram (d). Cutting it in the way presented in Fig. 3, we obtain the product of the tree-level and one-loop vertex amplitudes.²

Instead of calculating the spectral and statistical components of the self-energies, it is easier to calculate the Wightman components $\Sigma_{\geq}(x, y) \equiv \Sigma_F(x, y) \mp \frac{i}{2}\Sigma_\rho(x, y)$. These can be identified with the gain and loss terms, as mentioned earlier in this section. After some simple but tedious algebra (see Appendix C for more details), we obtain the self-energies corresponding to the diagrams in Fig. 1:

$$\Sigma_{\geq}^{(b)}(x, y) = -\frac{1}{2}\lambda^2 D_{\geq}(x, y) D_{\geq}(x, y) D_{\leq}(y, x), \quad (11a)$$

$$\Sigma_{\geq}^{(c)}(x, y) = -g_i g_j^* G_{\leq}^{ij}(y, x) D_{\leq}(y, x), \quad (11b)$$

$$\begin{aligned} \Sigma_{\geq}^{(d)}(x, y) = & -g_i g_j g_m^* g_n^* \int \mathcal{D}^4 v \mathcal{D}^4 u \\ & [D_R(y, v) D_F(u, v) D_{\leq}(u, x) G_R^{ij}(y, u) G_{\geq}^{mn}(x, v) \\ & + D_R(y, v) D_A(u, v) D_{\leq}(u, x) G_F^{ij}(y, u) G_{\geq}^{mn}(x, v) \\ & + D_F(y, v) D_R(u, v) D_{\leq}(u, x) G_R^{ij}(y, u) G_{\geq}^{mn}(x, v) \\ & + D_{\leq}(y, v) D_F(u, v) D_A(u, x) G_{\leq}^{ij}(y, u) G_R^{mn}(x, v) \\ & + D_{\leq}(y, v) D_A(u, v) D_F(u, x) G_{\leq}^{ij}(y, u) G_R^{mn}(x, v) \\ & + D_{\leq}(y, v) D_R(u, v) D_A(u, x) G_{\leq}^{ij}(y, u) G_F^{mn}(x, v) \\ & + D_R(y, v) D_{\geq}(u, v) D_A(u, x) G_{\leq}^{ij}(y, u) G_{\geq}^{mn}(x, v) \\ & + D_{\leq}(y, v) D_{\leq}(u, v) D_{\leq}(u, x) G_R^{ij}(y, u) G_R^{mn}(x, v)]. \quad (11c) \end{aligned}$$

Diagrams (b) and (c) in Fig. 1 induce contributions $\Sigma^{(b)}$ and $\Sigma^{(c)}$ which contain only the Wightman two-point correlation functions D_{\geq} and G_{\geq}^{ij} . As we will show later, in the Boltzmann approximation these correspond to the on-shell initial and final states. To write the last term in

compact form, we have introduced the retarded and advanced propagators, $D_R(x, y) \equiv \theta(x^0 - y^0) D_\rho(x, y)$ and $D_A(x, y) \equiv -\theta(y^0 - x^0) D_\rho(x, y)$, respectively. The first six terms³ of $\Sigma^{(d)}$ describe the one-loop correction to the decay width. The combinations of the statistical, retarded and advanced propagators in Eq. (11c) correspond to the three internal lines in the loop, whereas the \geq components again correspond to the on-shell initial and final states.

Since we do not consider quartic interactions of the real scalar fields, there are no local corrections to their masses. It is for this reason that Eqs. (9) contain only the bare masses M_i^2 of the fields. The first nonlocal term $\Pi^{(c)}$ describes the decay of the heavy scalar at tree-level:

$$\Pi_{\geq}^{(c)ij}(x, y) = -\frac{1}{2}g_i g_j^* D_{\geq}^2(x, y) - \frac{1}{2}g_i^* g_j D_{\leq}^2(y, x), \quad (12a)$$

$$\begin{aligned} \Pi_{\geq}^{(d)ij}(x, y) = & -\frac{1}{2}g_i g_j g_m^* g_n^* \int \mathcal{D}^4 v \mathcal{D}^4 u \\ & [G_F^{mn}(v, u) D_{\geq}(x, v) D_{\geq}(x, u) D_R(y, v) D_R(y, u) \\ & + G_R^{mn}(v, u) D_{\geq}(x, v) D_{\geq}(x, u) D_R(y, v) D_F(y, u) \\ & + G_A^{mn}(v, u) D_{\geq}(x, v) D_{\geq}(x, u) D_F(y, v) D_R(y, u) \\ & + G_F^{mn}(v, u) D_R(x, v) D_R(x, u) D_{\leq}(y, v) D_{\leq}(y, u) \\ & + G_R^{mn}(v, u) D_R(x, v) D_F(x, u) D_{\leq}(y, v) D_{\leq}(y, u) \\ & + G_A^{mn}(v, u) D_F(x, v) D_R(x, u) D_{\leq}(y, v) D_{\leq}(y, u) \\ & + G_{\leq}^{mn}(v, u) D_{\geq}(x, v) D_R(x, u) D_R(y, v) D_{\leq}(y, u) \\ & + G_{\leq}^{mn}(v, u) D_R(x, v) D_{\geq}(x, u) D_{\leq}(y, v) D_R(y, u)] \\ & - \frac{1}{2}g_i^* g_j^* g_m g_n \int \mathcal{D}^4 v \mathcal{D}^4 u \\ & [G_F^{mn}(v, u) D_{\leq}(v, x) D_{\leq}(u, x) D_A(v, y) D_A(u, y) \\ & + \dots] \quad (12b) \end{aligned}$$

The first six terms⁴ in each of the two square brackets of $\Pi^{(d)}$ describe the one-loop corrections to the scattering width. Their structure is very similar to that of the first six terms of Eq. (11c) and the combinations of the statistical, retarded and advanced propagators again correspond to the three internal lines in the loop.

The Kadanoff-Baym equations (8) and (9) together with the expression for the self-energies (11) and (12) form a closed system of integro-differential equations. Its solutions carry full information about the spectral and statistical properties of the system, including information about the generated asymmetry at each instant of time.

² In addition, there are two other ways to cut this diagram, which are denoted by the ellipses in Fig. 2. They describe scattering processes $bb \rightarrow \bar{b}\bar{b}$, $b\bar{b} \rightarrow \psi_i \psi_j$ and $\psi_i b \rightarrow \psi_j b$. Note that the three-loop 2PI diagram only describes the interference of the s , t and u -channel scattering amplitudes: M_{st} , M_{su} , M_{tu} . The missing topologies, which generate the M_{ss} , M_{tt} , and M_{uu} terms, appear only upon use of the *extended quasiparticle approximation*. This analysis is beyond the scope of this paper and will be presented in [29].

³ The seventh term in (11c) describes the scattering process $\psi_i b \rightarrow \psi_j b$. This is clear from the fact that it contains one D_{\geq} and two G_{\geq} two-point functions, i.e. one “external” complex scalar and two “external” real scalars. Similarly, the eighth term of Eq. (11c) describes the scattering process $b\bar{b} \rightarrow \bar{b}\bar{b}$, because it contains three D_{\geq} two-point functions, i.e. three “external” complex scalars.

⁴ The seventh and eighth terms of Eq. (12b) describe the scattering processes $\psi_i b \rightarrow \psi_j b$ and $b\bar{b} \rightarrow \psi_i \psi_j$.

B. Quantum-corrected Boltzmann equations

Despite all advantages, the full Kadanoff–Baym equations are relatively rarely used for the analysis of out-of-equilibrium processes, partially because of the complexity of the numerical solution.⁵ In this section we derive kinetic equations starting from the above Kadanoff–Baym equations by applying a gradient expansion and a quasiparticle approximation [31–34, 39, 49, 50]. The resulting quantum-corrected Boltzmann equations can be directly compared to the canonical equations and are easier to solve numerically.

The quantum-corrected Boltzmann equations are applicable to weakly coupled systems of (quasi)particles that have a width which is small compared to their mass and that evolves slowly compared to the microscopic interaction time scales. We expect that these conditions are satisfied for thermal leptogenesis, where the deviations from equilibrium are moderate in general. In thermal equilibrium the two-point correlation functions $D(x, y)$ and $G^{ij}(x, y)$ depend only on the relative coordinate, $s \equiv x - y$, and are independent of the center coordinate⁶, $X \equiv \frac{1}{2}(x + y)$. Having these equilibrium considerations in mind, we trade the variables x and y for the new arguments X and s : $D(x, y) \rightarrow D(X, s)$. Out of equilibrium the two-point functions depend on both the relative and center coordinate. If, however, the deviation from equilibrium is small, one can perform a gradient expansion of the correlation functions and the self-energies in the vicinity of X keeping only the leading terms. This results in a system of equations describing the slow, X -dependent dynamics of the statistical properties of the system, see Appendix B for more details. Performing the gradient expansion, which is the first step in the derivation of the Boltzmann equation, we replace the non-Markovian evolution equations by a system of Markovian ones. Therefore, when truncating at first order in the gradient expansion, we neglect the memory effects. The fast dynamics associated with the relative coordinate is responsible for the spectral properties of the system, which are conveniently described in the momentum representation. Performing the Wigner transformation (see Appendix B), we trade the relative coordinate s for a coordinate p in momentum space: $D(X, s) \rightarrow D(X, p)$. To perform the Wigner transformation we have to send the initial time to minus infinity which means that we neglect the effects of initial correlations. The next step in the derivation of Boltzmann equations is the Kadanoff–Baym *ansatz*. It relates the

statistical propagator and the spectral function by a generalized fluctuation-dissipation relation,

$$D_F(X, p) = [f(X, p) + \frac{1}{2}] D_\rho(X, p), \quad (13)$$

where $f(X, p)$ is the one-particle distribution function. In the equilibrium limit, the Kubo–Martin–Schwinger condition [52, 53] ensures that $f(X, p)$ converges towards a Bose–Einstein distribution function. The final step is the quasiparticle approximation, where one replaces the exact smooth spectral function by a Dirac δ function peaked on the mass-shell of the quasiparticles. The resulting Boltzmann-like equation, which describes the time evolution of the particle distribution function, reads

$$[p^\alpha \mathcal{D}_\alpha f(X, p)] D_\rho(X, p) = \frac{1}{2} [D_<(X, p) \Sigma_>(X, p) - D_>(X, p) \Sigma_<(X, p)]. \quad (14)$$

The analogous equation for antiparticles is given by

$$[p^\alpha \mathcal{D}_\alpha \bar{f}(X, p)] \bar{D}_\rho(X, p) = \frac{1}{2} [\bar{D}_<(X, p) \bar{\Sigma}_>(X, p) - \bar{D}_>(X, p) \bar{\Sigma}_<(X, p)], \quad (15)$$

where $\bar{D}_\geq(X, p) \equiv D_\leq(X, -p)$, $\bar{\Sigma}_\geq(X, p) \equiv \Sigma_\leq(X, -p)$.

Note again that by making the approximations which have led to (14) and (15) we have neglected the memory effects and the effects of the initial correlations. As a result, the quantum-corrected Boltzmann equations are Markovian, i.e. local in time.

To obtain a closed system of quantum-corrected Boltzmann equations, we must also Wigner-transform the self-energies (11) (see Appendix D for more details). The latter encode the scattering and decay rates including quantum nonequilibrium effects. By employing the relations

$$D_<(X, p) = f(X, p) D_\rho(X, p), \\ D_>(X, p) = [1 + f(X, p)] D_\rho(X, p),$$

which follow directly from Eq. (13), we can then rewrite Eqs. (14,15) in a way resembling the usual form of Boltzmann equations, including the correct quantum statistical factors.

Within the 2PI three-loop approximation, we find that there are two physically distinct contributions to the self-energy. The first one, corresponding to $\Sigma^{(b)}$, describes CP -conserving two body scatterings, $bb \rightarrow bb$, at tree-level:

$$\Sigma_{\geq}^\times(X, p) = -\frac{1}{2} \lambda^2 \int d\Pi_{p_1} d\Pi_{p_2} d\Pi_{p_3} (2\pi)^4 \delta^g(p + p_1 - p_2 - p_3) D_{\leq}(X, p_1) D_{\geq}(X, p_2) D_{\geq}(X, p_3), \quad (16)$$

where the invariant volume element in momentum space is defined by

$$d\Pi_p \equiv \frac{1}{\sqrt{-g_X}} \frac{d^4 p}{(2\pi)^4}, \quad (17)$$

and $\delta^g(p) \equiv \sqrt{-g_X} \delta(p)$ is the covariant generalization of the δ function [30].

⁵ See e.g. [40–48].

⁶ The above definitions of the relative and center coordinates are valid only in Minkowski space-time. In a general space-time the center coordinate is defined as coordinates of the center (ς_X) of the geodesic connecting x and y , $X^\alpha \equiv \xi^\alpha(\varsigma_X)$, whereas the relative coordinate is proportional to the length of the geodesic between the two points, $s^\alpha \equiv u^\alpha(\varsigma_X)(\varsigma_x - \varsigma_y)$ [51].

The second contribution, given by the sum of $\Sigma^{(c)}$ and $\Sigma^{(d)}$, describes decay processes $\psi_i \rightarrow b\bar{b}$ and $\psi_i \rightarrow \bar{b}b$ at tree- and one-loop level:

$$\Sigma_{\geq}^{(d)}(X, p) = -|g_i|^2 \int d\Pi_{p_1} d\Pi_{p_2} (2\pi)^4 \delta^g(p_1 - p_2 - p) \times [1 + \Delta_b^i(X, p_1, p_2)] G_{\geq}^{ii}(X, p_1) D_{\leq}(X, p_2). \quad (18)$$

The newly introduced function $\Delta_b^i(X, p_1, p_2)$ takes into account the one-loop corrections to the decay width and is given by

$$\begin{aligned} \Delta_b^i(X, p_1, p_2) = & |g_j|^2 \left(\frac{g_i g_j^*}{g_i^* g_j} \right) \int d\Pi_{k_1} d\Pi_{k_2} d\Pi_{k_3} \\ & \times (2\pi)^4 \delta^g(p_1 + k_1 + k_2) (2\pi)^4 \delta^g(k_2 - k_3 + p_2) \\ & \times [D_A(X, k_1) D_F(X, k_2) G_A^{jj}(X, k_3) \\ & + D_A(X, k_1) D_R(X, k_2) G_F^{jj}(X, k_3) \\ & + D_F(X, k_1) D_A(X, k_2) G_A^{jj}(X, k_3)] + \text{c.c.} \quad (19) \end{aligned}$$

Proceeding in the same way, we derive quantum-corrected Boltzmann equations for the distribution functions of the real scalar fields, which is a two-by-two differential matrix equation. The off-diagonal components of the correlation functions are generated dynamically by the exchange of two complex scalars and are therefore of order g^2 . The one-loop vertex terms, which generate the CP -violating parameter, are proportional to the fourth power of the coupling constant. Therefore the contribution of the off-diagonal terms to the vertex CP -violating parameter is of the order of g^6 . Here, we limit ourselves to terms of at most fourth power in the coupling constant and therefore we can neglect the off-diagonal terms in the corresponding matrix equation. The resulting equations coincide then with those derived in [30]:

$$\begin{aligned} [p^\alpha \mathcal{D}_\alpha f_{\psi_i}(X, p)] G_\rho^{ii}(X, p) \\ = \frac{1}{2} [G_{<}^{ii}(X, p) \Pi_{>}^{ii}(X, p) - G_{>}^{ii}(X, p) \Pi_{<}^{ii}(X, p)]. \quad (20) \end{aligned}$$

Note that we have in fact used this diagonal approximation in Eqs. (18) and (19). The Wigner-transform of the self-energy (12) is given in the same approximation by

$$\begin{aligned} \Pi_{\geq}^{ii}(X, p) = & -\frac{1}{2} |g_i|^2 \int d\Pi_{p_1} d\Pi_{p_2} (2\pi)^4 \delta^g(p_1 + p_2 - p) \\ & \times \{ [1 + \Delta_\psi^i(X, p, p_2)] D_{\geq}(X, p_1) D_{\geq}(X, p_2) \\ & + [1 + \bar{\Delta}_\psi^i(X, p, p_2)] \bar{D}_{\geq}(X, p_1) \bar{D}_{\geq}(X, p_2) \}. \quad (21) \end{aligned}$$

The second line of (21) describes the process $\psi \rightarrow b\bar{b}$. The one-loop correction to this process is given by

$$\begin{aligned} \Delta_\psi^i(X, p, p_2) = & |g_j|^2 \left(\frac{g_i g_j^*}{g_i^* g_j} \right) \int d\Pi_{k_1} d\Pi_{k_2} d\Pi_{k_3} \\ & \times (2\pi)^4 \delta^g(p + k_1 + k_2) (2\pi)^4 \delta^g(k_2 - k_3 + p_2) \\ & \times [D_R(X, k_1) D_R(X, k_2) G_F^{jj}(X, k_3) \\ & + D_R(X, k_1) D_F(X, k_2) G_A^{jj}(X, k_3) \\ & + D_F(X, k_1) D_R(X, k_2) G_R^{jj}(X, k_3)] + \text{c.c.} \quad (22) \end{aligned}$$

The third line of (21) describes $\psi \rightarrow \bar{b}b$ process and the corresponding one-loop contribution is related to (22) by $\bar{\Delta}_\psi^i(X, p_1, p_2) \equiv \Delta_\psi^i(X, -p_1, -p_2)$.

A very important feature of the expressions for the self-energies, Eqs. (18) and (21), is that the loop corrections Δ_b^i and Δ_ψ^i appear as overall factors on the right-hand sides of the corresponding quantum-corrected Boltzmann equations. Therefore, when using the conventional approximations and integrating Eqs. (14,15), we obtain the structure⁷

$$\partial_t(n_b, n_{\bar{b}}) \propto (1 \pm \epsilon_i)(n_i - n_i^{eq}) \dots \quad (23)$$

To obtain an equivalent result in the canonical approach one explicitly needs to apply the RIS subtraction procedure. This means that, here, the structure of the equations automatically ensures that no asymmetry is generated in thermal equilibrium. Stated differently, the Kadanoff–Baym formalism is *free of the double-counting problem* and no need for RIS subtraction arises.

In the homogeneous and isotropic early universe the canonical Boltzmann equations conserve the linear combination $2n_{\psi_i} + n_b + n_{\bar{b}}$ of particle numbers in a comoving volume. However, the conservation of this quantity is accidental, i.e. not guaranteed by a symmetry of the underlying Lagrangian. It is not conserved by the full Kadanoff–Baym equations⁸ (see [47] for another example). This is also true for the *quantum-corrected Boltzmann equations* which we have derived from the Kadanoff–Baym equations. To see this one should add Eqs. (14) and (15) as well as Eq. (20) multiplied by two and use the explicit expressions for the self-energies (18) and (21). Although the expressions for the loop corrections (19) and (22) are similar, they are not equal. This results in a small time-dependence of the quantity mentioned above (see also Appendix G).

The system of Boltzmann equations (14), (15) and (20) together with the Wigner-transforms of the self-energies (16), (18) and (21) form a closed system of differential equations that can be solved numerically. The solutions describe the phase-space distributions of quasiparticle excitations at each instant of time $t = X^0$.

⁷ For the numerical analysis we use the full Boltzmann equation, since the approximations required to obtain integrated rate equations are not appropriate within the toy model (see Sec. IV). Note, however, that the latter in fact contain *averaged* effective CP -violating parameters (see Sec. III and Appendix F), $\epsilon_i \rightarrow \langle \epsilon_i \rangle$.

⁸ It is important to note that the 2PI approximation scheme guarantees that the total *energy-momentum tensor* (including “potential” energy due to interactions in the system) is covariantly conserved [33, 54]. In other words, the nonconservation of the total number of particles does not violate the fundamental conservation laws.

III. CP -VIOLATING PARAMETER

Comparing the Boltzmann equations for particles and antiparticles, (14) and (15), we see that the dynamical generation of the CP asymmetry is only possible if $\Sigma_{\geq}(X, p) \neq \Sigma_{\leq}(X, p)$. Since $\Sigma_{\geq}(X, p) \equiv \Sigma_{\leq}(X, -p)$, in the diagonal approximation, this is equivalent to the requirement that $\Delta_b^i(X, p_1, p_2) \neq \Delta_b^i(X, -p_1, -p_2)$. The CP -violating parameter can then be defined as

$$\epsilon_i(X, p_1, p_2) \equiv \frac{1}{2}[\Delta_b^i(X, p_1, p_2) - \Delta_b^i(X, -p_1, -p_2)]. \quad (24)$$

Using properties of the Wigner transforms of the statistical, retarded and advanced propagators, we find that in a medium that is (approximately) baryosymmetric⁹ it is given by

$$\begin{aligned} \epsilon_i(X, p_1, p_2) = & |g_j|^2 \text{Im} \left(\frac{g_i g_j^*}{g_i^* g_j} \right) \int d\Pi_{k_1} d\Pi_{k_2} d\Pi_{k_3} \\ & \times (2\pi)^4 \delta^g(p_1 + k_1 + k_2) (2\pi)^4 \delta^g(k_2 - k_3 + p_2) \\ & \times [D_\rho(X, k_1) D_F(X, k_2) G_h^{jj}(X, k_3) + \{k_1 \leftrightarrow k_2\} \\ & + D_h(X, k_1) D_F(X, k_2) G_\rho^{jj}(X, k_3) + \{k_1 \leftrightarrow k_2\} \\ & + D_\rho(X, k_1) D_h(X, k_2) G_F^{jj}(X, k_3) - \{k_1 \leftrightarrow k_2\}], \quad (25) \end{aligned}$$

where $D_h(X, p) \equiv \text{Re} D_R(X, p) = \text{Re} D_A(X, p)$ and G_h is defined analogously. The quasiparticle approximation together with the Kadanoff–Baym ansatz enforces the spectral functions and the statistical propagators to be on mass-shell. On the contrary, the real parts of the retarded propagators, D_h and G_h , vanish on-shell (see Appendix B for more detail). In other words, in the pro-

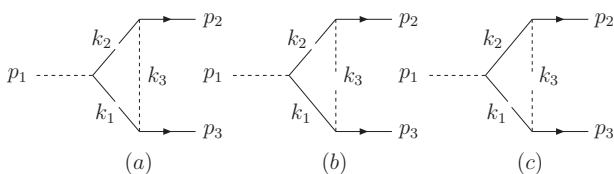


FIG. 4: Graphical representation of the terms in Eq. (25).

cesses contributing to the CP -violating parameter, two of the intermediate lines are on-shell and one line is off-shell; this is shown in Fig. 4. It is also interesting to note that in each term on the right-hand side of (25) only one of the internal lines is “thermal”, i.e. explicitly depends on the one-particle distribution function. In

other words the medium corrections are only *linear* in the particle number densities. One could come to this conclusion even without explicitly calculating the CP -violating parameter. The self-energy (11c) is a product of five two-point correlation functions. As far as the decay is concerned, two of them describe on-shell “external” states. The two integrals over the space-time coordinates, u and v , turn two other functions into retarded and (or) advanced propagators, which do not explicitly depend on the particle number densities. The remaining function turns out to be given by the corresponding statistical propagator and explicitly depends on the particle number density.

Typically, one is interested only in the total generated asymmetry and solves rate equations for the total particle number densities. They are obtained by integrating the left- and right-hand sides of the Boltzmann equations (14) and (15) over phase space. In the corresponding gain and loss terms,

$$\begin{aligned} & \int d\Pi_p d\Pi_{p_1} d\Pi_{p_2} (2\pi)^4 \delta^g(p_1 - p_2 - p) [1 \pm \epsilon_i(X, p_1, p_2)] \\ & \times G_{\geq}^{ii}(X, p_1) D_{\leq}(X, p_2) D_{\leq}(X, p), \quad (26) \end{aligned}$$

we can perform the transformation $p \leftrightarrow p_2$ and take a sum of the initial and final expressions, so that in Eq. (26):

$$\epsilon_i(X, p_1, p_2) \rightarrow \frac{1}{2}[\epsilon_i(X, p_1, p_2) + \epsilon_i(X, p_1, p)]. \quad (27)$$

In $\epsilon_i(X, p_1, p)$, we transform the variables $k_1 \leftrightarrow k_2$ and $k_3 \rightarrow -k_3$ in addition. The spectral function of a real scalar field is antisymmetric: $G_\rho^{ii}(X, -k_1) = -G_\rho^{ii}(X, k_1)$. Collecting all the terms, we find that due to the antisymmetry only the first two terms (the third line) in (25) contribute to the right-hand side of (27), whereas the other terms cancel out. In other words, only the first two terms of (25) contribute to the total CP -asymmetry, whereas the other four terms do not. An explicit calculation shows that (at least in the homogeneous and isotropic universe) these four terms also do not contribute to the gain and loss terms. Diagrammatically this means that only decays followed by a scattering contribute to the CP -violating parameter, see Fig. 4a.

As we have already mentioned, it is important that the CP -violating parameters ϵ_i are identical¹⁰ for the gain and the loss terms: this means that the structure of the quantum-corrected Boltzmann equation automatically ensures that the asymmetry vanishes in thermal equilibrium. Let us also note that there is a clear distinction between the initial, final and intermediate states: the former ones are described by the Wightman functions

⁹ We will see later that the CP -violating parameter, defined in this way, is different for particles and antiparticles if the corresponding distribution functions are different. Since the expected asymmetry is small, this is only a second order effect and can be neglected in the present work. The condition of almost zero asymmetry is certainly satisfied if the CP -violating parameter is calculated in vacuum, as it is the case in the canonical approach.

¹⁰ It is important to note that the transformation properties under C , P and T of the self-energies obtained from the Schwinger–Keldysh/Kadanoff–Baym formalism cannot be identified with those of the S -Matrix elements appearing in the canonical in-out formalism.

D_{\geq} and G_{\geq} , whereas the latter ones are described by the retarded, advanced and (or) statistical components of the two-point functions.

Applying the quasiparticle approximation and the Kadanoff–Baym ansatz in Eq. (25), we obtain the following expression for the CP -violating parameter which is one of our central results:

$$\epsilon_i(p_1, p_2) = -\frac{1}{8\pi} \frac{|g_j|^2}{M_i^2} \text{Im} \left(\frac{g_i g_j^*}{g_i^* g_j} \right) \times \int \frac{d\Omega}{4\pi} \frac{1 + \bar{f}(E_{k_1}) + \bar{f}(E_{k_2})}{M_j^2/M_i^2 + \frac{1}{2}(1 + \cos\theta)}, \quad (28)$$

where $E_{k_{1,2}}$ are the energies of the intermediate toy baryons as a function of p_1 , p_2 and the angle variables, and we have omitted the time-space coordinate X to shorten the notation. The CP -violating parameter is a sum of vacuum and medium contributions. Integrating the vacuum contribution over the solid angle, we obtain the standard expression for the CP -violating parameter, see Eq. (2). The thermal contributions are proportional to the one-particle distribution function, which is positive. Hence, for scalars the CP -violating parameter is always *enhanced* by the medium effects.

Because of the fact that the intermediate toy baryons propagate with respect to the rest frame of the thermal bath, the CP -violating parameter depends in each individual decay on the phase-space distribution of the decaying particle and the decay products. Using results of Appendix E, we obtain for the energy of the intermediate complex scalars:

$$E_{k_{1,2}} = \frac{1}{2}[E_1 + |\mathbf{p}_1|(\sin\theta \cos\varphi \cos\delta' \mp \cos\theta \sin\delta')], \quad (29)$$

where θ and φ are elements of the solid angle Ω and the angle δ' depends on momenta of the initial and final states: $\sin\delta' = (|\mathbf{p}_3| - |\mathbf{p}_2|)/|\mathbf{p}_1|$.

In the limit of almost equal one-particle distribution functions of particles and antiparticles, f and \bar{f} , the CP -violating parts of Δ_{ψ}^i do not contribute to the Boltzmann equations for the real scalars, just as in the canonical approach. For this reason, we do not consider it here.

In order to estimate the size of the medium corrections, we consider the hierarchical limit of the heavy scalar mass spectrum, $M_1 \ll M_2$. As in standard leptogenesis, we assume that the asymmetry is predominantly generated by the decay of the lighter scalar. By expanding Eq. (28) in M_1^2/M_2^2 , we obtain a simplified expression for the relevant CP -violating parameter ϵ_1 ,

$$\epsilon_1(p_1, p_2) = \epsilon_1^{vac} \left[1 + \int \frac{d\Omega}{4\pi} \{ \bar{f}(E_{k_1}) + \bar{f}(E_{k_2}) \} \right], \quad (30)$$

where ϵ_1^{vac} is the CP -violating parameter in vacuum given in Eq. (2). Exploiting the $k_1 \leftrightarrow k_2$ symmetry and integrating over the full solid angle we find that the asymmetry depends on the absolute value of \mathbf{p}_1 only. That is $\epsilon_1(p_1, p_2) = \epsilon_1(|\mathbf{p}_1|)$, where

$$\epsilon_1(|\mathbf{p}|) = \epsilon_1^{vac} \left[1 + \frac{2}{r|\mathbf{p}|} \int_{E_{min}/2}^{E_{max}/2} \bar{f}(E) dE \right], \quad (31)$$

and $E_{max} = E_1 + r|\mathbf{p}|$ and $E_{min} = E_1 - r|\mathbf{p}|$ are the largest and smallest kinematically allowed energies of the light scalars produced in the decay $\psi_1 \rightarrow b\bar{b}$. Here $E_1 = (M_1^2 + \mathbf{p}^2)^{\frac{1}{2}}$ and $|\mathbf{p}|$ denote the energy and momentum of ψ_1 in the rest frame of the medium, respectively. Furthermore, we have also included a nonzero “baryon” mass m for completeness, which enters via the parameter $r \equiv (1 - 4m^2/M_1^2)^{\frac{1}{2}}$.

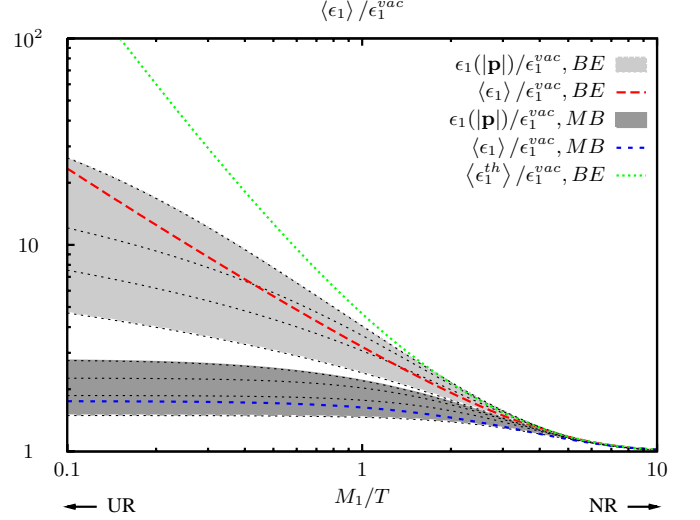


FIG. 5: Effective CP -violating parameter $\epsilon_1(|\mathbf{p}|)$ in medium obtained from the Kadanoff–Baym formalism. The shaded areas correspond to the range $0.25 \leq |\mathbf{p}|/T \leq 4$ of momenta $|\mathbf{p}|$ of the decaying particle $\psi_1 \rightarrow b\bar{b}/b\bar{b}$ with respect to the rest frame of the medium. Here we assumed a thermal Bose-Einstein (BE) and Maxwell-Boltzmann (MB) distribution for b/\bar{b} with vanishing chemical potential for illustration. In the low-temperature limit (NR), the vacuum value is approached. In the high-temperature limit (UR), the CP -violating parameter is enhanced for bosons. We also show the thermally averaged CP -violating parameter $\langle \epsilon_1 \rangle$ for the BE (red long-dashed line) and MB (blue dashed line) cases, as well as the result that would be obtained in thermal field theory (green dotted line).

The medium correction depends on the one-particle distribution function of the light scalars and the masses of the particles. As expected they vanish if $\bar{f} \equiv 0$. We emphasize that the upper expression is valid even if the light scalars were out of equilibrium. Nevertheless, since we expect the light scalars to be close to kinetic equilibrium at all times, we insert a Bose–Einstein distribution function. For comparison we also consider the case of a Maxwell–Boltzmann distribution. Then we obtain

$$\frac{\epsilon_1(|\mathbf{p}|)}{\epsilon_1^{vac}} = 1 + \frac{2T}{r|\mathbf{p}|} \times \begin{cases} \ln \left(\frac{1 - \exp\left(-\frac{E_{max}-2\mu}{2T}\right)}{1 - \exp\left(-\frac{E_{min}-2\mu}{2T}\right)} \right) & \text{BE} , \\ e^{-\frac{E_{min}-2\mu}{2T}} - e^{-\frac{E_{max}-2\mu}{2T}} & \text{MB} . \end{cases} \quad (32)$$

The resulting expression depends on time $t = X_0$ via temperature T and chemical potential μ of the toy baryons.

For the rest of this section we assume $|\mu| \ll T$, as in realistic scenarios of leptogenesis, for the purpose of illustration¹¹. The temperature and momentum dependence of the medium correction in the range of typical momenta $|\mathbf{p}| \sim T$ is shown in the shaded areas in Fig. 5 for the BE and MB cases, respectively. It is instructive to consider the nonrelativistic (NR) regime ($T, |\mathbf{p}| \ll M_1$) and the ultrarelativistic (UR) regime ($T \gtrsim |\mathbf{p}| \gg M_1$). In the nonrelativistic (NR) limit, the BE and MB cases coincide, and the medium correction is exponentially suppressed,

$$\epsilon_1(|\mathbf{p}|)/\epsilon_1^{vac} \rightarrow 1 + 2 \exp\left(-\frac{M_1}{2T}\right). \quad (33)$$

Furthermore, it is independent of the momentum $|\mathbf{p}|$. In the UR limit, the medium correction for the BE and MB cases behaves quite differently: In the MB case the medium correction saturates at $\epsilon_1/\epsilon_1^{vac} \lesssim 3$. In the BE case, it is logarithmically enhanced¹² (see Fig. 5),

$$\epsilon_1(|\mathbf{p}|)/\epsilon_1^{vac} \rightarrow 1 + \frac{2T}{r|\mathbf{p}|} \ln\left(\frac{4T|\mathbf{p}|}{M_1^2 + \frac{8\mathbf{p}^2 m^2}{M_1^2(1+r)}}\right). \quad (34)$$

This effect is due to Bose enhancement. Thus, we find that the quantum statistics is important for the medium correction. In the following section, we will see that the logarithmic enhancement at high energies is also suppressed by the inclusion of sizable negative chemical potentials (which is necessary within the toy model, see below). In Fig. 5, we also show the CP -violating parameter $\langle\epsilon_1\rangle$ obtained from averaging Eq. (32) over the momentum $|\mathbf{p}|$ (see Appendix F). As expected, $\langle\epsilon_1\rangle \sim \epsilon_1(|\mathbf{p}| \sim T)$.

Before discussing the impact of the medium correction quantitatively, we would like to comment on the relation between the Kadanoff-Baym (top-down) and the canonical (bottom-up) approach. As has been mentioned before, *in vacuum*, the top-down result Eq. (28) for the CP -violating parameter coincides with the canonical result Eq. (2). Nevertheless, we emphasize again that the structure of the Boltzmann equations differs between the two approaches, i.e. the former are free of the double-counting problem. Furthermore, it is also important to note that the size of the medium correction differs between the top-down and the bottom-up approach.

Within the latter, the medium corrections have been discussed by replacing $\epsilon_i^{vac} \rightarrow \epsilon_i^{th}$ in the canonical Boltzmann equations. Hereby ϵ_i^{th} involves the vertex loop calculated within thermal field theory (see e.g. [19, 20]). For the toy model, ϵ_i^{th} is given in Eq. (A5) of Appendix A. It involves an additional term compared to the top-down result (28), which is quadratic in the particle distribution function. In Fig. 5 we show that the medium correction would be significantly over-estimated in the canonical thermal field theory approach within the toy model.

For realistic models of leptogenesis, the vertex loop contains scalar and fermionic lines in general. In contrast to the scalars, the latter tend to *decrease* the size of the CP -violating parameter. Therefore the results shown here can only be used indirectly to make statements for phenomenology. For the standard scenario of thermal leptogenesis with hierarchical right-handed neutrino spectrum, it has been observed in [19] that, within thermal field theory, the effects of Bose enhancement and Pauli blocking tend to cancel each other. However, since the medium corrections differ within the Kadanoff-Baym formalism, this cancellation may no longer occur. Therefore one might expect that the medium correction is underestimated in this case, contrary to the situation encountered within the toy model discussed here.

Note that we have neglected the effect of thermal masses here for simplicity. Their impact on leptogenesis has been studied e.g. in [20] within the framework of thermal field theory. For the toy model considered here, it is consistent to neglect thermal masses due to the absence of gauge interactions. We stress, however, that it is also possible to include time-dependent effective masses systematically within the Kadanoff-Baym formalism. One of the effects caused by the thermal masses of the complex field is the cutoff of the logarithmic enhancement of the CP -violating parameter at high energies. In addition, in an asymmetric medium the effective masses of the particles and antiparticles are not equal, which leads to an effective CP violation. This effect is studied in [55]. The medium corrections to the masses of the heavy real fields can be important in the case of the degenerate mass spectrum, which we investigate in [29].

Since the quantum statistic is important for the CP -violating parameter in medium, we also have to include the quantum statistical terms in the gain and loss terms of the Boltzmann equations for consistency. This will be discussed in the following section.

IV. NUMERICAL RESULTS

To obtain the three Boltzmann equations for f , \bar{f} and f_{ψ_1} , we integrate each of Eqs. (14), (15) and (20) over p_0 (left- and right-hand side) and choose the positive energy solution [30]. In agreement with the cosmological principle, we solve the system of Boltzmann equations with spatially homogeneous and momentum isotropic distribution functions in (flat and radiation dominated)

¹¹ In realistic scenarios, the leptons and Higgs fields are in equilibrium with gauge bosons such that $\mu = -\bar{\mu}$. The smallness of the asymmetry then ensures the smallness of the chemical potentials, $|\mu|/T = |\bar{\mu}|/T \sim 10^{-10}$. Within the toy model, due to the absence of gauge interactions, it is possible to have $|\mu| \simeq |\bar{\mu}| \sim T$ while the asymmetry remains small. It turns out that this is even necessary to obtain consistent numerical solutions within the present scenario, see Sec. IV.

¹² Note that the logarithmic enhancement at high energies is cut-off for extremely high energies ($|\mathbf{p}| \gg M_1^2/m$) in the UV due to the second summand of the denominator inside the logarithm. Since we assume that $m \ll M_1/10$, we can neglect this term in the relevant temperature range $M_1/T > 0.1$.

Friedman–Robertson–Walker (FRW) space-time. In this case the left-hand side of the Boltzmann equation is given by

$$L[f](|\mathbf{p}|) \equiv p^\alpha \mathcal{D}_\alpha f(|\mathbf{p}|) = p^0 \left(\frac{\partial}{\partial t} - |\mathbf{p}| H \frac{\partial}{\partial |\mathbf{p}|} \right) f(|\mathbf{p}|), \quad (35)$$

where $H \equiv \dot{a}/a$ is the Hubble parameter. Since in the quasiparticle approximation the spectral functions

are proportional to $\delta(p^2 - m^2)$, the integration over the time components of the quasiparticle's four-momenta can be performed trivially in each of the corresponding self-energies. After the integration the volume element $d\Pi_p$ is replaced by $d\Pi_p^3 \equiv d^3p/(2\pi)^3/2E$, where E is energy of the on-shell quasiparticle.

With these modifications, the network of quantum-corrected Boltzmann equations takes the form:

$$L[f](|\mathbf{p}|) = C_{bb \leftrightarrow bb}[f](|\mathbf{p}|) + C_{b\bar{b} \leftrightarrow b\bar{b}}[f, \bar{f}](|\mathbf{p}|) + C_{bb \leftrightarrow \psi_1}[f, f_{\psi_1}](|\mathbf{p}|), \quad (36a)$$

$$L[\bar{f}](|\mathbf{p}|) = C_{b\bar{b} \leftrightarrow b\bar{b}}[\bar{f}](|\mathbf{p}|) + C_{b\bar{b} \leftrightarrow b\bar{b}}[\bar{f}, f](|\mathbf{p}|) + C_{b\bar{b} \leftrightarrow \psi_1}[\bar{f}, f_{\psi_1}](|\mathbf{p}|), \quad (36b)$$

$$L[f_{\psi_1}](|\mathbf{p}|) = C_{\psi_1 \leftrightarrow bb}[f_{\psi_1}, f](|\mathbf{p}|) + C_{\psi_1 \leftrightarrow b\bar{b}}[f_{\psi_1}, \bar{f}](|\mathbf{p}|), \quad (36c)$$

where the different collision terms for the transition between two states i and f are denoted by $C_{i \leftrightarrow f}$. Note that, due to the isotropy of the FRW universe, the collision terms also depend only on the absolute value of the momenta. For the $2-2$ scattering processes in (36a) we find

$$C_{bb \leftrightarrow bb}[f](|\mathbf{p}|) = \frac{1}{2} \int d\Pi_{p_2}^3 d\Pi_{p_3}^3 d\Pi_{p_4}^3 (2\pi)^4 \delta^{(4)}(p + p_2 - p_3 - p_4) \times \frac{1}{2} \lambda^2 \{ [1 + f(|\mathbf{p}|)] [1 + f(|\mathbf{p}_2|)] f(|\mathbf{p}_3|) f(|\mathbf{p}_4|) - f(|\mathbf{p}|) f(|\mathbf{p}_2|) [1 + f(|\mathbf{p}_3|)] [1 + f(|\mathbf{p}_4|)] \}, \quad (37a)$$

$$C_{b\bar{b} \leftrightarrow b\bar{b}}[f, \bar{f}](|\mathbf{p}|) = \frac{1}{2} \int d\Pi_{p_2}^3 d\Pi_{p_3}^3 d\Pi_{p_4}^3 (2\pi)^4 \delta^{(4)}(p + p_2 - p_3 - p_4) \times \lambda^2 \{ [1 + f(|\mathbf{p}|)] [1 + \bar{f}(|\mathbf{p}_2|)] \bar{f}(|\mathbf{p}_3|) f(|\mathbf{p}_4|) - f(|\mathbf{p}|) \bar{f}(|\mathbf{p}_2|) [1 + \bar{f}(|\mathbf{p}_3|)] [1 + f(|\mathbf{p}_4|)] \}. \quad (37b)$$

The corresponding terms in the equation for \bar{b} can be obtained by replacing f with \bar{f} in (37a) and (37b). If the generated asymmetry is small, as we assume here, then $f \approx \bar{f}$. In this case the CP-violating contributions to the right-hand side of (36c) cancel out and we obtain:

$$C_{\psi_1 \leftrightarrow bb}[f_{\psi_1}, f](|\mathbf{p}|) + C_{\psi_1 \leftrightarrow b\bar{b}}[f_{\psi_1}, \bar{f}](|\mathbf{p}|) \simeq \frac{1}{2} \int d\Pi_{p_2}^3 d\Pi_{p_3}^3 (2\pi)^4 \delta^{(4)}(p - p_2 - p_3) \times \frac{1}{2} |g_1|^2 \{ ([1 + f_{\psi_1}(|\mathbf{p}|)] f(|\mathbf{p}_2|) f(|\mathbf{p}_3|) - f_{\psi_1}(|\mathbf{p}|) [1 + f(|\mathbf{p}_2|)] [1 + f(|\mathbf{p}_3|)] + [1 + f_{\psi_1}(|\mathbf{p}|)] \bar{f}(|\mathbf{p}_2|) \bar{f}(|\mathbf{p}_3|) - f_{\psi_1}(|\mathbf{p}|) [1 + \bar{f}(|\mathbf{p}_2|)] [1 + \bar{f}(|\mathbf{p}_3|)] \}. \quad (38)$$

The collision terms for the (inverse) decay of the heavy particle into a bb or $b\bar{b}$ pair explicitly contain the CP-violating parameter ϵ defined in Eq. (31):

$$C_{bb \leftrightarrow \psi_1}[f, f_{\psi_1}](|\mathbf{p}|) = \frac{1}{2} \int d\Pi_{p_2}^3 d\Pi_{p_3}^3 (2\pi)^4 \delta^{(4)}(p_2 - p - p_3) \times |g_1|^2 [1 + \epsilon_1(|\mathbf{p}_2|)] \{ [1 + f(|\mathbf{p}|)] [1 + f(|\mathbf{p}_3|)] f_{\psi_1}(|\mathbf{p}_2|) - f(|\mathbf{p}|) f(|\mathbf{p}_3|) [1 + f_{\psi_1}(|\mathbf{p}_2|)] \} \quad (39a)$$

$$C_{b\bar{b} \leftrightarrow \psi_1}[\bar{f}, f_{\psi_1}](|\mathbf{p}|) = \frac{1}{2} \int d\Pi_{p_2}^3 d\Pi_{p_3}^3 (2\pi)^4 \delta^{(4)}(p_2 - p - p_3) \times |g_1|^2 [1 - \epsilon_1(|\mathbf{p}_2|)] \{ [1 + \bar{f}(|\mathbf{p}|)] [1 + \bar{f}(|\mathbf{p}_3|)] f_{\psi_1}(|\mathbf{p}_2|) - \bar{f}(|\mathbf{p}|) \bar{f}(|\mathbf{p}_3|) [1 + f_{\psi_1}(|\mathbf{p}_2|)] \}. \quad (39b)$$

The factors $1/2$ associated with the couplings in (37a) and (38) correctly account for the symmetrization of collision integrals which include integration over the momenta of two identical particles in the initial/final state. They have been consistently obtained in the derivation from the Kadanoff–Baym equations. We would like to stress again that the structure of (39) differs from the usual structure obtained in the conventional bottom-up approach. In particular, we do not need to include col-

lision terms for the processes $bb \leftrightarrow b\bar{b}$ (not even the RIS part of it) because our collision terms for the processes $bb \leftrightarrow \psi_1$ and $b\bar{b} \leftrightarrow \psi_1$ do not suffer from the generation of an asymmetry in equilibrium. The network of Boltzmann equations (36) should be understood in the generalized sense: the “amplitudes” differ from the usual perturbative matrix elements and do not have their symmetry properties.

To stay consistent in our model we also keep the quan-

tum statistical factors for bosons. The implications of this new structure for a phenomenological theory of leptogenesis will be discussed elsewhere. To study the effect of the quantum corrections, we compare the results obtained by integrating the network of Boltzmann equations with quantum-corrected $\epsilon_1(|\mathbf{p}|)$ to those which are obtained after replacing $\epsilon_1(|\mathbf{p}|)$ with ϵ_1^{vac} . This means that we keep here the new structure of the Boltzmann equations and study corrections which arise from the quantum-corrected ϵ_1 only. In the vacuum limit the structure of Eq. (36) corresponds to the one which has been assumed implicitly in [56] if the quantum statistical factors and the symmetrization factor are replaced accordingly.

In both cases we start at sufficiently high temperatures so that all species, including ψ_1 with mass $M_1 = 10^{10}$ GeV, have relativistic initial abundances which corresponds to the most frequently discussed case.¹³ Because of the presence of the statistical factors we need to start with sufficiently negative chemical potentials as to avoid Bose–Einstein condensation of the different species during their evolution.¹⁴ We choose them such that they are related by $\mu_{\psi_1} = 2\mu_b = 2\mu_{\bar{b}}$, i.e. the system is in chemical equilibrium.

The coupling λ can be adjusted such that the rates of the $2-2$ interactions (37) are much larger than those of the decays and inverse decays (38)–(39) at all times¹⁵. This keeps b and \bar{b} close to kinetic equilibrium, just as Higgs particles and leptons are kept in equilibrium by rapid gauge interactions in the standard scenario. The distribution functions for these species are therefore given by their equilibrium form throughout the entire evolution. This means that they can be described in terms of four parameters μ_b , T_b and $\mu_{\bar{b}}$, $T_{\bar{b}}$. The interactions (37) enforce the relation $T_{\bar{b}} = T_b$ between the parameters. Therefore, it is sufficient to study the evolution of f and \bar{f} in terms of the remaining three parameters (see Appendix G). The evolution of ψ_1 , however, is studied in terms of the complete distribution function discretized on a grid with 400 momentum modes. Our computation, therefore, includes classical nonequilibrium effects in the

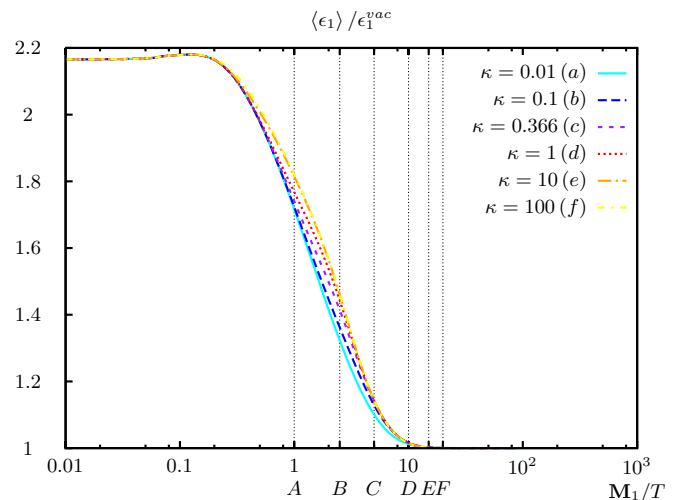


FIG. 6: The ratio $\langle \epsilon_1 \rangle / \epsilon_1^{vac}$. The shape of the curves differs from that of the corresponding graph in Fig. 5, mainly because its computation involves a finite chemical potential (which depends on M_1/T here). Similar graphs can be obtained by including a finite chemical potential in Eq. (32).

decay of ψ_1 . Such effects have been studied recently in [56–58]. All integrals are evaluated numerically including all quantum statistical factors for stimulated emission.

We define the generated “baryon” asymmetry as

$$\eta(M_1/T) = \frac{n_b(M_1/T) - n_{\bar{b}}(M_1/T)}{s(M_1/T)}. \quad (40)$$

Here n_b and $n_{\bar{b}}$, the number densities of species b and \bar{b} respectively (compare (G7)), are computed in the presence of the quantum-corrected ϵ_1 , and s is the standard entropy density [1]. The analogous asymmetry computed with ϵ_1^{vac} is denoted by $\eta^{vac}(M_1/T)$.

Figure 6 shows the numerical value of the ratio $\langle \epsilon_1 \rangle / \epsilon_1^{vac}$ for various values of the washout parameter $\kappa \equiv \Gamma/H(M_1) = |g_1|^2 m_{pl} / (4.5 \cdot 16\pi \sqrt{g_*} M_1^3)$. The flattening for small M_1/T as compared to the thermal equilibrium result in Fig. 5 is due to the finite chemical potential of \bar{b} . This shows that larger corrections could be obtained if additional interactions for b and \bar{b} are introduced which would allow one to start with smaller chemical potentials and hence lead to a stronger enhancement.

The buildup of the asymmetry with and without quantum corrections as a function of the inverse temperature is depicted in Figs. 7 and 8. Comparing these figures one can verify the enhancement of the asymmetry at intermediate stages for larger washout factors (case d). Note also that due to the medium contribution to the CP -violating parameter the generated asymmetry is not a monotonous function of the washout parameter κ .

The dependence of the resulting final asymmetries $\eta = \eta(M_1/T \rightarrow \infty)$ and $\eta^{vac} = \eta^{vac}(M_1/T \rightarrow \infty)$ as well as the ratio $(\eta - \eta^{vac})/\eta^{vac}$ on the washout parameter is presented in Fig. 9. The asymmetry is always larger when

¹³ Another scenario, which is frequently discussed in the literature, is that the Majorana neutrinos could have zero initial abundance. In this case we would expect the differences in the time evolution of the asymmetry to be larger in general. However, this can have an effect on the final asymmetry only if the asymmetry, produced in the intermediate step of thermalization, is not washed out again before the Majorana neutrinos decouple, i.e. for small washout factor $\kappa \lesssim 1$.

¹⁴ In this regime it would not be appropriate to describe the system by conventional Boltzmann kinetic equations. Since we are interested in scenarios that are qualitatively similar to realistic models of leptogenesis here, we do not consider this case.

¹⁵ As we will show in Appendix G in this case there is no need to compute the collision integrals for $2-2$ scattering explicitly and we can use perturbative values for λ for most of the relevant range of $|g|^2$ assuming that it is sufficient to demand that the rate for $b\bar{b} \leftrightarrow \psi_1$ is at least 10^3 times larger than that of $b\bar{b} \leftrightarrow \psi_1$.

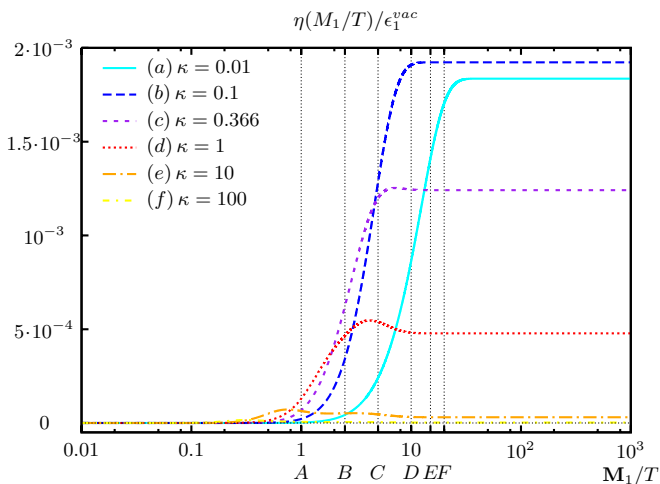


FIG. 7: The asymmetry $\eta(M_1/T)$ with quantum corrections included. In the weak washout regime (case *a*) the asymmetry is produced at smaller temperatures and it is not necessarily larger than for larger washout factors (compare *a* and *b*).

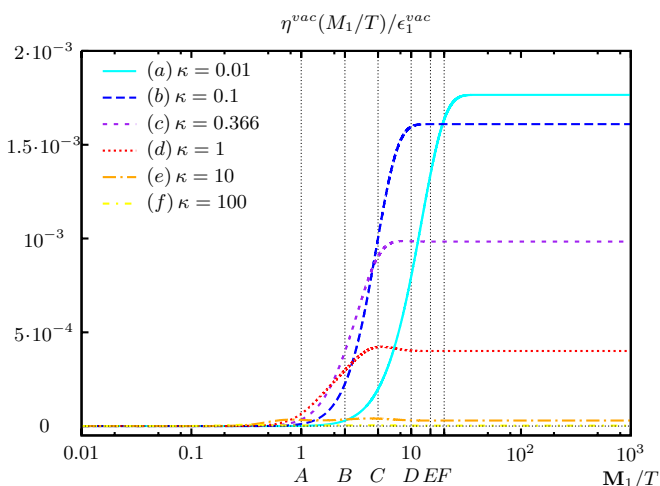


FIG. 8: The asymmetry $\eta^{vac}(M_1/T)$ without quantum corrections.

quantum corrections are taken into account compared to the results without corrections (compare Sec. III). The asymmetry η has a maximum for moderate washout factors $\kappa \simeq 0.059$ in contrast to the usual result which has its maximum in the limit of zero washout factor. Our interpretation of this result is as follows: For large washout factors the enhancement of ϵ_1 due to the quantum corrections enhances the asymmetry generated by the decays only at intermediate stages, because the same processes diminish the asymmetry in particular at late times where the averaged asymmetry drops to smaller values (compare Fig. 6). For small κ the particles decay late, and the backreaction is largely suppressed so that the washout is ineffective. However the interval of integration in Eq. (31) is located at relatively large momenta since the mass in-

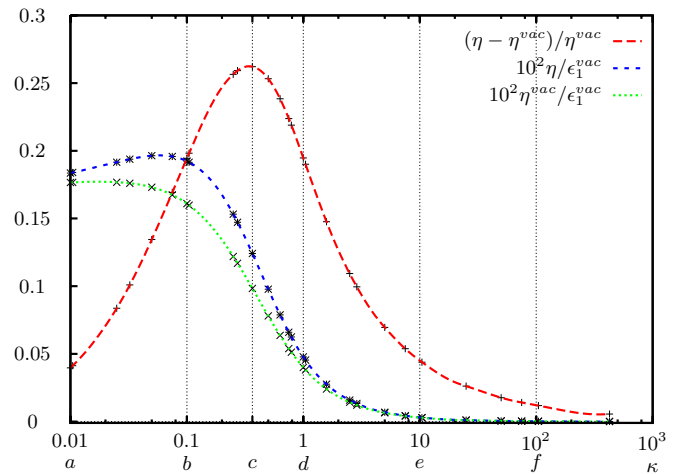


FIG. 9: The final asymmetries and the ratio $(\eta - \eta^{vac})/\eta^{vac}$ over washout factor κ . The cases *a*, *b*, *c*, *d*, *e*, *f* correspond to washout factors 0.01, 0.1, 0.366, 1, 10, 100. Case *c* is close to the maximum relative excess of the quantum-corrected results at $\kappa \simeq 0.34$. In contrast to the usual results the final asymmetry does not take its maximum value for the smallest washout factor. Instead, the asymmetry η peaks at $\kappa \simeq 0.059$.

creasingly dominates $E_1 = (M_1^2 + \mathbf{p}^2)^{1/2}$ as the momenta are redshifted to smaller values. This means that the integration is over an interval in which the distribution \bar{f} becomes smaller and smaller. This explains why the quantum corrections tend to zero for small κ . For the same reasons the relative effect of the quantum corrections peaks at a moderate $\kappa \simeq 0.34$ with about 26%.

We note again that the size and the sign of the corrections depend on the quantum statistics of the particles in the vertex loop and will be different in a phenomenological scenario. Further plots and details about the numerical algorithm can be found in Appendix G.

V. CONCLUSIONS AND OUTLOOK

In this paper, we have studied leptogenesis in a simple toy model consisting of one complex and two real scalar fields in a top-down approach, using the Schwinger–Keldysh/Kadanoff–Baym formalism as the starting point. This treatment, based on nonequilibrium quantum field theory techniques, is motivated by the fact that it allows a unified description of two key ingredients of leptogenesis, namely deviation from thermal equilibrium and loop-induced CP violation. It has several important advantages in comparison to the canonical bottom-up (Boltzmann) approach. In particular, the full Kadanoff–Baym equations do not rely on the concept of quasiparticles and their collisions in the plasma. However, if the quasiparticle picture is applicable, as we have assumed here, the Kadanoff–Baym formalism consistently accounts for the dependence of the quasiparticles' properties as well as scattering and decay rates on

the state of the medium.

The out-of-equilibrium dynamics of the quasiparticles is described by a system of approximate self-consistent kinetic equations – *quantum-corrected Boltzmann equations* – which we have derived here starting from the full system of the Kadanoff–Baym equations. We find that the structure of the quantum-corrected Boltzmann equations automatically ensures that no asymmetry is produced in thermal equilibrium. In other words there is no need for the real intermediate state subtraction, i.e. the formalism is free of the double-counting problem typical for the canonical approach.

One of the key quantities in leptogenesis is the CP -violating parameter. Earlier studies have shown that there are two sources of CP violation: self-energy and vertex contributions. In this work, we have concentrated on the latter one. We have found that for scalar fields the medium effects increase the vertex contribution to the CP -violating parameter. At high temperatures it is up to an order of magnitude larger than in vacuum and asymptotically approaches the vacuum value as the temperature decreases. This result can be traced back to a Bose enhancement of the vertex loop correction. In the Maxwell–Boltzmann approximation, the corresponding CP -violating parameter is increased at most by a factor two. We would also like to note that, in the vacuum limit, the CP -violating parameter obtained via the Kadanoff–Baym formalism agrees with the value obtained within the canonical formalism, as expected.

It is interesting that, contrary to the results obtained earlier in the framework of thermal field theory by replacing the zero-temperature propagators with finite temperature propagators in the matrix elements of the Boltzmann equation, the medium corrections depend only linearly on the particle number densities. Stated differently, only one of the internal lines in the vertex loop is “thermal”. Moreover, the medium corrections to the vertex CP -violating parameter depend only on the density of the toy baryons and are independent of the density of the “Majorana” particles. Since the decaying heavy particles as well as the intermediate on-shell states propagate with respect to the thermal bath’s rest frame, the CP -violating parameter in each individual decay depends on the momenta of the initial and final states.

We have solved the system of the *quantum-corrected Boltzmann equations* numerically. Because of the medium corrections to the CP -violating parameter the asymmetry reaches its maximum value at a small but finite value of the washout parameter κ , rather than for $\kappa \rightarrow 0$, as it is the case in the canonical approach. To avoid the regime of Bose–Einstein condensation we have to assume that the species have rather large chemical potentials initially. This decreases the medium correction to the CP -violating parameter. As a result the generated asymmetry differs from its value in the canonical formalism by approximately 26%. However, in a scenario in which the chemical potentials are close to zero the deviation could reach the 100% level. As has been mentioned

above, our results differ from the results of the calculations performed in vacuum and in the framework of thermal field theory. Therefore, we argue that one should use the quantum-corrected Boltzmann equations (or the full Kadanoff–Baym equations). On the other hand, to obtain order of magnitude approximations, it seems safe to use the canonical approach in the present scenario.

The techniques described in this work can also be used to study quantum nonequilibrium effects within phenomenological scenarios of leptogenesis. In particular, the technical advantages of the Kadanoff–Baym formalism demonstrated above, like the absence of double-counting problems, are quite generic and therefore should not depend on the details of the model. Furthermore, we expect that the difference in the size of the medium corrections, obtained from the Kadanoff–Baym formalism and thermal field theory respectively, persists if our approach is applied to such scenarios.

We would like to stress again that, in this paper, we have considered only the vertex contribution to the CP -violating parameter. The self-energy contribution is comparable to the vertex contribution or, in the case of resonant leptogenesis, considerably larger than the vertex contribution. We will study it in a forthcoming paper [29]. In addition in [55] we plan to investigate the influence of a nonzero asymmetry on the CP -violating parameter. Furthermore, for phenomenological models, thermal masses can become relevant. These can also consistently be described within the Kadanoff–Baym formalism. Finally, we note that it would also be interesting to investigate numerical solutions of the full set of Kadanoff–Baym equations without further approximations as some of their properties cannot be included in Boltzmann-like equations for principle reasons. This is however beyond the scope of the present work.

Acknowledgements

This work was supported by the “Sonderforschungsbereich” TR27 and by the “cluster of excellence Origin and Structure of the Universe”. We would like to thank J.-S. Gagnon for useful discussions and M. M. Müller for sharing his insights on nonequilibrium field theory.

Appendix A: CP -violating parameter in the bottom-up approach

In this appendix, we review the calculation of the vertex contribution to the CP -violating parameter in vacuum, $\epsilon_i^{vac} \equiv (\Gamma_{\psi_i \rightarrow bb} - \Gamma_{\psi_i \rightarrow \bar{b}\bar{b}}) / (\Gamma_{\psi_i \rightarrow bb} + \Gamma_{\psi_i \rightarrow \bar{b}\bar{b}})$, in the conventional in-out formalism. It is generated by the interference of the tree-level and one-loop amplitudes (see

Fig. 3),

$$\begin{aligned}\mathcal{M}_{\psi_i \rightarrow bb}^{(0)} &= -ig_i^*, \\ \mathcal{M}_{\psi_i \rightarrow bb}^{(1)} &= ig_i g_j^* g_j^* \frac{1}{16\pi^2} C_0(M_i^2, 0, M_j^2).\end{aligned}$$

In the limit of massless toy baryons, the scalar 1-loop vertex three-point function C_0 is given by [59, 60]:

$$C_0(p_1^2, p_2^2, M_j^2) = \int \frac{(i\pi^2)^{-1} d^4 q}{(q^2 - M_j^2)(q + p_2)^2(q + p_2 - p_1)^2}, \quad (\text{A2})$$

where p_1 and p_2 are momenta of the decaying heavy particle and of one of the decay products, respectively. The tree-level and one-loop amplitudes of the decay process $\psi \rightarrow \bar{b}b$ differ from (A1) only by conjugation of the couplings. Therefore, at leading order, we obtain for the CP -violating parameter:

$$\epsilon_i^{vac} = \frac{|g_j|^2}{8\pi^2} \text{Im} \left(\frac{g_i g_j^*}{g_i^* g_j} \right) \text{Im} C_0(M_i^2, 0, M_j^2). \quad (\text{A3})$$

Substituting the result for the three-point function,

$$C_0(M_i^2, 0, M_j^2) = \frac{1}{M_i^2} \left[\text{Li}_2 \left(1 + \frac{M_i^2}{M_j^2} \right) - \frac{\pi^2}{6} \right], \quad (\text{A4})$$

(with dilogarithm Li_2 as defined in [60]) into Eq. (A3), we obtain Eq. (2). The same calculation can be performed within thermal quantum field theory by using thermal propagators in Eq. (A2). The result is [19, 53]

$$\begin{aligned}\epsilon_i^{th}(p_1, p_2) &= -\frac{1}{8\pi} \frac{|g_j|^2}{M_i^2} \text{Im} \left(\frac{g_i g_j^*}{g_i^* g_j} \right) \\ &\times \int \frac{d\Omega}{4\pi} \frac{1 + \bar{f}_1^{th} + \bar{f}_2^{th} + 2\bar{f}_1^{th}\bar{f}_2^{th}}{M_j^2/M_i^2 + \frac{1}{2}(1 + \cos\theta)} + \dots, \quad (\text{A5})\end{aligned}$$

where $\bar{f}_i^{th} = [\exp((E_{k_i} - \mu)/T) - 1]^{-1}$, see Eq. (29). The ellipsis denote similar contributions involving the distribution function of the heavy scalar. These are suppressed in the hierarchical limit.

Appendix B: Kadanoff–Baym formalism for the complex scalar field

Here, we derive the Kadanoff–Baym and quantum-corrected Boltzmann equations for the complex scalar field.

1. Schwinger–Dyson equation

Our starting point is the generating functional for Green’s functions [61]:

$$\mathcal{Z}[J, K] = \int \mathcal{D}b \mathcal{D}\bar{b} \exp[i(S + \bar{J}b + \bar{J}\bar{b} + \bar{b}Kb)], \quad (\text{B1})$$

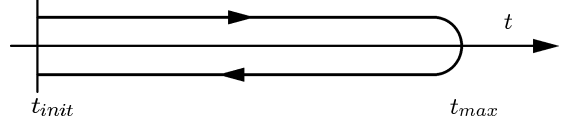


FIG. 10: Closed real-time path \mathcal{C} .

where the field and the external sources are defined on the the positive and negative branches of the Schwinger–Keldysh closed real-time contour shown in Fig. 10 [31, 62–66]. The scalar products of the local and bilocal sources $J(x)$ and $K(x, y)$ and the field are defined as invariant configuration space integrals [30, 67]. Furthermore, we use the compact notation of Ref. [31] for contour integrals over the closed real-time path. Note that the sources are now complex functions. The requirement that the last term in (B1) be real implies that $K(x, y) = K^*(y, x)$.

The functional derivatives of the generating functional for connected Green’s functions,

$$\mathcal{W}[J, K] = -i \ln \mathcal{Z}[J, K], \quad (\text{B2})$$

with respect to the external sources read

$$\frac{\partial \mathcal{W}[J, K]}{\partial J(x)} = \bar{B}(x), \quad (\text{B3a})$$

$$\frac{\partial \mathcal{W}[J, K]}{\partial K(x, y)} = \frac{1}{2} [D(y, x) + \bar{B}(x)B(y)]. \quad (\text{B3b})$$

B and D denote the expectation value and the propagator of the field respectively. The derivative of \mathcal{W} with respect to \bar{J} is just the complex conjugate of (B3a).

Performing a Legendre transform of the generating functional for connected Green’s functions, we obtain the effective action

$$\Gamma[D, B] \equiv \mathcal{W}[J, K] - J\bar{B} - \bar{J}B - \text{tr}[KD] - \bar{B}KB. \quad (\text{B4})$$

Making use of the chain rule and Eqs. (B3), we find for functional derivatives of the effective action

$$\frac{\delta \Gamma[D, B]}{\delta \bar{B}(x)} = -J(x) - \int \mathcal{D}^4 z K(x, z)B(z), \quad (\text{B5a})$$

$$\frac{\delta \Gamma[D, B]}{\delta D(x, y)} = -K(y, x). \quad (\text{B5b})$$

Next, we shift the complex field by its expectation value $b \rightarrow b + B$. Since the integration measure in the path integral is translationally invariant, the effective action can be rewritten in the form

$$\begin{aligned}\Gamma[D, B] &= -i \ln \int \mathcal{D}b \mathcal{D}\bar{b} \exp[i(S + \bar{J}b + \bar{J}\bar{b} + \bar{b}Kb)] \\ &\quad + S_{cl}[B] - \text{tr}[KD].\end{aligned} \quad (\text{B6})$$

Now, we tentatively write the effective action in the form [61]

$$\begin{aligned}\Gamma[D, B] &\equiv S_{cl}[B] + i \ln \det [D^{-1}] + i \text{tr} [\mathcal{D}^{-1}D] \\ &\quad + \Gamma_2[D, B],\end{aligned} \quad (\text{B7})$$

thus defining the functional Γ_2 .

The third term on the right-hand side of (B7) is given by a convolution of the field propagator D and the free inverse propagator \mathcal{D}^{-1} . Its differentiation with respect to $D(y, x)$ gives [30]

$$\mathcal{D}^{-1}(x, y) = i(\square_x + m^2) \delta^g(x, y). \quad (\text{B8})$$

The functional derivative of the second term on the right-hand side of (B7) can be obtained upon use of

$$\int \mathcal{D}^4 z D^{-1}(x, z) D(z, y) = \delta^g(x, y), \quad (\text{B9})$$

and is given by $-iD^{-1}(y, x)$. Consequently, we obtain

$$\begin{aligned} \frac{\delta \Gamma[D, B]}{\delta D(x, y)} &= -iD^{-1}(y, x) + i\mathcal{D}^{-1}(y, x) + \frac{\delta \Gamma_2[D, B]}{\delta D(x, y)} \\ &= -K(y, x). \end{aligned} \quad (\text{B10})$$

Physical reality corresponds to vanishing sources.¹⁶ Therefore, Eq. (B10) can be rewritten in the form

$$D^{-1}(x, y) = \mathcal{D}^{-1}(x, y) - \Sigma(x, y), \quad (\text{B11})$$

where the self-energy is defined by

$$\Sigma(x, y) \equiv i \frac{\delta \Gamma_2[D, B]}{\delta D(y, x)}. \quad (\text{B12})$$

Note that the factor two in the definition of the self-energy [30, 47] is absent, just as one would expect for a complex field.

2. Kadanoff–Baym equations

Convolving the Schwinger–Dyson equation (B11) with D from the right and using Eq. (B9), we obtain

$$\begin{aligned} i[\square_x + m^2]D(x, y) &= \delta_g(x, y) \\ &+ \int \mathcal{D}^4 z \Sigma(x, z) D(z, y). \end{aligned} \quad (\text{B13})$$

Next, following the usual procedure, we represent the time-ordered propagator as a linear combination of the statistical propagator and spectral function:

$$D(x, y) = D_F(x, y) - \frac{i}{2} \text{sign}_C(x^0 - y^0) D_\rho(x, y), \quad (\text{B14})$$

where sign_C denotes the signum function with respect to time ordering along the closed time path, and

$$D_F(x, y) \equiv \frac{1}{2} \langle [b(x), \bar{b}(y)]_+ \rangle, \quad (\text{B15a})$$

$$D_\rho(x, y) \equiv i \langle [b(x), \bar{b}(y)]_- \rangle, \quad (\text{B15b})$$

where the subscripts “+” and “−” denote the anticommutator and the commutator of the fields.

To find out how D_F and D_ρ behave under complex conjugation let us introduce

$$D_{>}(x, y) \equiv \langle b(x) \bar{b}(y) \rangle = \text{Tr}[\mathcal{P} b(x) \bar{b}(y)], \quad (\text{B16a})$$

$$D_{<}(x, y) \equiv \langle \bar{b}(y) b(x) \rangle = \text{Tr}[\mathcal{P} \bar{b}(y) b(x)]. \quad (\text{B16b})$$

Using the Hermiticity of the density matrix \mathcal{P} and the cyclic invariance of the trace, we obtain

$$D_{>}^*(x, y) = D_{>}(y, x), \quad D_{<}^*(x, y) = D_{<}(y, x). \quad (\text{B17})$$

Consequently

$$D_F^*(x, y) = D_F(y, x), \quad D_\rho^*(x, y) = -D_\rho(y, x). \quad (\text{B18})$$

Analogous relations also hold for the spectral and statistical components of the self-energy.

The local part of the self-energy is proportional to the Dirac δ function and can be absorbed in the effective mass of the field, $m^2(x) \equiv m^2 + \Sigma^{\text{loc}}(x, x)$, whereas the remaining part of the self-energy can be split into a spectral part Σ_ρ and a statistical part Σ_F in a complete analogy to (B14).

Because of the sign function, the action of the Laplace–Beltrami operator on (B14) gives rise to a product of $g^{00} \delta(x^0, y^0)$ and $\nabla_0^x D_\rho(x, y)$. Upon use of the definition of the spectral function and canonical commutation relations for a complex scalar field this product reduces to the generalized δ function $\delta^g(x, y)$ [30], which cancels the δ function on the right-hand side of (B13).

Separating spectral and statistical components in Eq. (B13), we obtain a system of Kadanoff–Baym equations very similar to that for the real scalar field [30]:

$$\begin{aligned} [\square_x + m^2(x)] D_F(x, y) &= \int_0^{y^0} \mathcal{D}^4 z \Sigma_F(x, z) D_\rho(z, y) \\ &- \int_0^{x^0} \mathcal{D}^4 z \Sigma_\rho(x, z) D_F(z, y), \end{aligned} \quad (\text{B19})$$

$$[\square_x + m^2(x)] D_\rho(x, y) = \int_{x^0}^{y^0} \mathcal{D}^4 z \Sigma_\rho(x, z) D_\rho(z, y). \quad (\text{B20})$$

One should, however, keep in mind that the functions in (B19) and (B20) are *complex*. That is, we get four equations for the real and imaginary components of the spectral function and the statistical propagator. The complete information about the (Gaussian) initial state specified at the initial time $t_{\text{init}} \equiv 0$ enters via the initial conditions of the two-point functions D_F , $\partial_{x^0} D_F$, $\partial_{y^0} D_F$ and $\partial_{x^0} \partial_{y^0} D_F$ evaluated at $x^0 = y^0 = t_{\text{init}}$. The corresponding initial conditions for the spectral function are fixed by the equal-time commutation relation of the complex field, as for the real case [38].

We note that the proper renormalization of the Kadanoff–Baym equations (B19, B20) would require one to also take non-Gaussian correlations of the initial

¹⁶ To be precise, within nonequilibrium field theory, this is only true for times $x^0, y^0 > t_{\text{init}}$. The local and bi-local sources supported at $x^0 = y^0 = t_{\text{init}}$ formally encode the information about the (Gaussian) initial state (see e.g. [38]). However, these sources do not appear explicitly in the Kadanoff–Baym equations, and therefore we omit them here.

state into account [68, 69]. However, the derivation of quantum-corrected Boltzmann equations considered here involves the limit $t_{init} \rightarrow -\infty$, and therefore the initial correlations should have a negligible effect.

3. Quantum kinetics

The Kadanoff–Baym equation for the statistical propagator (spectral function) can be rewritten in terms of the advanced and retarded propagators, D_R and D_A :

$$[\square_x + m^2(x)]D_{F(\rho)}(x, y) = -\int \mathcal{D}^4 z \theta(z^0) \times [\Sigma_{F(\rho)}(x, z)D_A(z, y) + \Sigma_R(x, z)D_{F(\rho)}(z, y)]. \quad (\text{B21})$$

Because of (B18), the retarded and advanced propagators are related by

$$D_R(x, y) \equiv \theta(x^0 - y^0)D_\rho(x, y) = -\theta(x^0 - y^0)D_\rho^*(y, x) = D_A^*(y, x). \quad (\text{B22})$$

Therefore, after interchange of x and y in (B21) and complex conjugation of the resulting equation, we find

$$[\square_y + m^2(y)]D_{F(\rho)}(x, y) = -\int \mathcal{D}^4 z \theta(z^0) \times [D_R(x, z)\Sigma_{F(\rho)}(z, y) + D_{F(\rho)}(x, z)\Sigma_A(z, y)]. \quad (\text{B23})$$

Since (B23) has been obtained from (B21) by reversible transformations, a solution of (B21) is also a solution of (B23). Consequently, it is also a solution of the sum (which will be referred to as *constraint* equation) and the difference (which will be referred to as *kinetic* equation) of (B21) and (B23).

To analyze the constraint and kinetic equations it is convenient to introduce the center and relative coordinates, X and s [51]. In terms of the center and relative coordinates relations (B18) can be rewritten in the form

$$D_F^*(X, s) = D_F(X, -s), \quad D_\rho^*(X, s) = -D_\rho(X, -s).$$

Consequently, even in the case of a complex scalar field, the Wigner transforms of the spectral function and statistical propagator,

$$D_F(X, p) = \sqrt{-g_X} \int d^4 s e^{ips} D_F(X, s), \quad (\text{B24a})$$

$$D_\rho(X, p) = -i\sqrt{-g_X} \int d^4 s e^{ips} D_\rho(X, s), \quad (\text{B24b})$$

are real-valued functions. The Wigner transforms of the retarded and advanced propagators are defined analogously to (B24a). From (B22) it then follows that relation

$$D_A(X, p) = D_R^*(X, p) \quad (\text{B25})$$

also holds for a complex scalar field. Another very useful relation,

$$D_R(X, p) - D_A(X, p) = iD_\rho(X, p), \quad (\text{B26})$$

results from the definitions (B22) and (B24) and the equality $\theta(s^0) + \theta(-s^0) = 1$. Equations (B25) and (B26) in particular imply that

$$D_{R(A)}(X, p) = D_h(X, p) \pm \frac{i}{2}D_\rho(X, p), \quad (\text{B27})$$

where $D_h(X, p) \equiv \text{Re } D_R(X, p)$ has been introduced. A similar relation also holds for the retarded and advanced self-energies.

Let us now subtract (B23) from (B21) and then Wigner transform the left- and right-hand sides of the resulting equation. Furthermore, we send the initial time to the infinite past, $t_{init} \rightarrow -\infty$, i.e. we drop the functions $\theta(z^0)$ on the right-hand sides of Eqs. (B21) and (B23). Physically, this means that we neglect the effects of initial correlations. Additionally, we perform a gradient expansion with respect to the central coordinate X . Proceeding as in [30], we obtain a kinetic equation for the spectral function. To linear order in the gradients it reads

$$\{\omega(X, p), D_\rho(X, p)\}_{PB} = \{\Sigma_\rho(X, p), D_h(X, p)\}_{PB}, \quad (\text{B28})$$

where we have introduced

$$\omega(X, p) \equiv g^{\mu\nu} p_\mu p_\nu - m^2(X) - \Sigma_h(X, p), \quad (\text{B29})$$

and the Poisson brackets are defined by [30]

$$\{A(X, p), B(X, p)\}_{PB} \equiv \frac{\partial}{\partial p_\alpha} A(X, p) \mathcal{D}_\alpha B(X, p) - \mathcal{D}_\alpha A(X, p) \frac{\partial}{\partial p_\alpha} B(X, p). \quad (\text{B30})$$

Wigner transforming the sum of (B23) and (B21), we obtain the constraint equation for the spectral function. To linear order in the gradients it is an *algebraic* equation:

$$\omega(X, p)D_\rho(X, p) = \Sigma_\rho(X, p)D_h(X, p). \quad (\text{B31})$$

To close the system and to analyze the spectrum, we also need the equations for the retarded and advanced propagators. They can be obtained from (B21) and (B23) upon use of the definitions of D_R and D_A and the canonical commutation relations:

$$[\square_x + m^2(x)]D_{R(A)}(x, y) = \delta^g(x, y) - \int \mathcal{D}^4 z \Sigma_{R(A)}(x, z)D_{R(A)}(z, y), \quad (\text{B32})$$

$$[\square_y + m^2(y)]D_{A(R)}(x, y) = \delta^g(x, y) - \int \mathcal{D}^4 z D_{A(R)}(x, z)\Sigma_{A(R)}(z, y). \quad (\text{B33})$$

Wigner transforming the *difference* of (B32) and (B33) and subtracting (B28), we obtain the kinetic equation for real part of the retarded and advanced propagators:

$$\{\omega(X, p), D_h(X, p)\}_{PB} = -\frac{1}{4}\{\Sigma_\rho(X, p), D_\rho(X, p)\}_{PB}. \quad (\text{B34})$$

Wigner transforming the *sum* of (B32) and (B33) and subtracting (B31), we obtain the second constraint equation:

$$\omega(X, p)D_h(X, p) = -1 - \frac{1}{4}\Sigma_\rho(X, p)D_\rho(X, p). \quad (\text{B35})$$

The solution of the system of constraint equations (B31) and (B35) reads

$$D_\rho(X, p) = \frac{-\Sigma_\rho(X, p)}{\omega^2(X, p) + \frac{1}{4}\Sigma_\rho^2(X, p)}, \quad (\text{B36a})$$

$$D_h(X, p) = \frac{\omega(X, p)}{\Sigma_\rho(X, p)} D_\rho(X, p). \quad (\text{B36b})$$

As can be checked by substitution, solution (B36) is also solution of the *kinetic* equations (B28) and (B34). In other words, to linear order in the gradients we have analytic expressions for the spectral function and retarded (advanced) propagators. The spectral function has a sharp peak on the mass shell, i.e. for $\omega(X, p) = 0$. The height and exact shape of the peak are time-dependent.

Proceeding in a similar way, we can derive the kinetic

$$\{\omega(X, p), D_F(X, p)\}_{PB} = \{\Sigma_F(X, p), D_h(X, p)\}_{PB} + D_F(X, p)\Sigma_\rho(X, p) - \Sigma_F(X, p)D_\rho(X, p), \quad (\text{B37})$$

and the constraint,

$$\omega(X, p)D_F(X, p) = \frac{1}{4}\{\Sigma_F(X, p), D_\rho(X, p)\}_{PB} \quad (\text{B38}) + \frac{1}{4}\{D_F(X, p), \Sigma_\rho(X, p)\}_{PB} + \Sigma_F(X, p)D_h(X, p)$$

equations for the statistical propagator. The constraint equation is no longer algebraic and cannot be, generally speaking, solved analytically. However, if the system is in thermal equilibrium, then all the quantities are constant in time and space and the Poisson brackets in (B38) vanish identically. The solution of the resulting equation reads

$$D_F^{eq}(p) = \frac{\Sigma_F(p)}{\Sigma_\rho(p)} D_\rho^{eq}(p). \quad (\text{B39})$$

That is, we have obtained the fluctuation-dissipation relation from the constraint equation (B38). As can be checked by substitution, in equilibrium (B39) is indeed a solution of (B37). Furthermore, using (B14) and the Kubo-Martin-Schwinger periodicity condition we find [38]

$$D_F^{eq}(p) = [f^{eq}(p) + \frac{1}{2}] D_\rho^{eq}(p), \quad (\text{B40})$$

where f^{eq} is the Bose-Einstein distribution function.

4. Quantum-corrected Boltzmann equations

The spectral function for the complex scalar field (B36a) has a Breit-Wigner shape and peaks at $\omega = 0$. The height of the peak is inversely proportional to the spectral self-energy and tends to infinity in the limit of vanishing coupling constant. Since, furthermore, the area under $D_\rho(X, p)$ is constant [30] to a first approximation it can be replaced by a Dirac δ function:

$$D_\rho(X, p) = 2\pi \text{sign}(p_0) \delta(g_{\mu\nu}p^\mu p^\nu - m^2). \quad (\text{B41})$$

Equation (B41) is referred to as *quasiparticle approximation*.

Strictly speaking, the quasiparticle approximation is sufficient only for the analysis of lowest-order processes. In the model under consideration this includes the tree-level decay and tree-level scattering processes, which are obtained at the order $\mathcal{O}(g^2)$ and $\mathcal{O}(\lambda^2)$, respectively (see Fig. 2). To ensure the consistency of the description beyond leading order one should use the so-called *extended quasiparticle approximation* [70–75]. The extended quasiparticle approximation for the complex scalar field would allow us, for instance, to describe $\psi b \rightarrow b \rightarrow \psi b$ scattering processes, which are of order $\mathcal{O}(g^4)$. In this paper we are primarily interested in the three-loop vertex diagram, whose contribution to the effective action contains the fourth power of the coupling g . Using the quasiparticle approximation for the propagators in the vertex diagram thus induces contributions which are already of order $\mathcal{O}(g^4)$. Consequently, the extended quasiparticle approximation would additionally induce contributions of higher order in the coupling constants. Therefore, the calculation of the leading order contribution to the vertex CP -violating parameter does not require us to go beyond the quasiparticle approximation.

As has been argued in [30], in the same approximation one can also neglect the Poisson brackets in the kinetic equations, which physically corresponds to the *Stosszahlansatz* of Boltzmann. This leads to a simple kinetic equation for the spectral function:

$$p^\alpha \mathcal{D}_\alpha D_\rho(X, p) = 0. \quad (\text{B42})$$

Let us note, that the quasiparticle approximation for the spectral function (B41) is consistent with (B42).

Neglecting the Poisson brackets on the right-hand side of (B37), we obtain the Boltzmann equation for the statistical propagator:

$$p^\alpha \mathcal{D}_\alpha D_F(X, p) = \frac{1}{2}[D_F(X, p)\Sigma_\rho(X, p) - \Sigma_F(X, p)D_\rho(X, p)]. \quad (\text{B43})$$

Motivated by the fluctuation-dissipation relation (B40), we trade the statistical propagator for the one-particle number density:

$$D_F(X, p) = [f(X, p) + \frac{1}{2}] D_\rho(X, p). \quad (\text{B44})$$

In view of (B42), we can then rewrite (B43) as an equation for the phase-space distribution function $f(X, p)$:

$$[p^\alpha \mathcal{D}_\alpha f(X, p)] D_\rho(X, p) = \frac{1}{2}[\Sigma_>(X, p)D_<(X, p) - D_>(X, p)\Sigma_<(X, p)], \quad (\text{B45})$$

where we have introduced

$$D_\gtrless(X, p) = D_F(X, p) \pm \frac{1}{2}D_\rho(X, p). \quad (\text{B46})$$

Equation (B45) is very similar to the Boltzmann equation for a real scalar field [30]. There is, however, an important difference. For negative values of p_0 the distribution

function f describes *antiparticles*:

$$f(X, -p) \equiv -[\bar{f}(X, p) + 1]. \quad (\text{B47})$$

In other words, Eq. (B45) describes the time evolution of both particles and antiparticles. One can obtain an explicit equation for f by changing the sign of p_0 :

$$\begin{aligned} [p^\alpha \mathcal{D}_\alpha \bar{f}(X, p)] D_\rho(X, p) \\ = \frac{1}{2} [\bar{\Sigma}_>(X, p) \bar{D}_<(X, p) - \bar{D}_>(X, p) \bar{\Sigma}_<(X, p)], \end{aligned} \quad (\text{B48})$$

where we have introduced $\bar{\Sigma}_\geq(X, p) \equiv \Sigma_\leq(X, -p)$ and taken into account that in the quasiparticle approximation $D_\rho(X, -p) = -D_\rho(X, p)$.

Appendix C: Calculation of the self-energies

The 2PI effective action is given by the sum of all 2PI diagrams with vertices as given by the interaction Lagrangian and internal lines representing the complete connected propagators [38]. The structure of the terms of the effective action can be read off the diagrams in Fig. 1:

$$i\Gamma_2^{(a)} = -\frac{i}{2} \lambda \int_x D^2(x, x), \quad (\text{C1a})$$

$$i\Gamma_2^{(b)} = -\frac{1}{8} \lambda^2 \int_{xy} D^2(x, y) D^2(y, x), \quad (\text{C1b})$$

$$\begin{aligned} i\Gamma_2^{(c)} = & -\frac{1}{4} g_m g_n^* \int_{xy} G^{mn}(x, y) D^2(x, y) \\ & -\frac{1}{4} g_m^* g_n \int_{xy} G^{mn}(x, y) D^2(y, x), \end{aligned} \quad (\text{C1c})$$

$$\begin{aligned} i\Gamma_2^{(d)} = & \frac{1}{4} g_i g_j g_m^* g_n^* \int_{xyvu} G^{ij}(x, y) G^{mn}(v, u) \\ & \times D(y, v) D(x, v) D(y, u) D(x, u), \end{aligned} \quad (\text{C1d})$$

where, to shorten the notation, we have introduced

$$\int_{x_1 \dots x_n} \equiv \int \mathcal{D}^4 x_1 \dots \mathcal{D}^4 x_n.$$

The self-energies of the complex scalar field are obtained by functional differentiation of the effective action with respect to the two-point correlation function:

$$\Sigma(x, y) \equiv i \frac{\delta \Gamma_2[D, G]}{\delta D(y, x)}. \quad (\text{C2})$$

Differentiating the individual contributions to the effective action, we obtain

$$\Sigma^{(a)}(x, y) = -i \delta^g(x, y) \lambda D(x, x), \quad (\text{C3a})$$

$$\Sigma^{(b)}(x, y) = -\frac{1}{2} \lambda^2 D^2(x, y) D(y, x), \quad (\text{C3b})$$

$$\Sigma^{(c)}(x, y) = -g_i g_j^* G^{ij}(y, x) D(y, x), \quad (\text{C3c})$$

$$\begin{aligned} \Sigma^{(d)}(x, y) = & g_i g_j g_m^* g_n^* \int_{vu} G^{mn}(x, v) G^{ij}(y, u) \\ & \times D(y, v) D(u, v) D(u, x). \end{aligned} \quad (\text{C3d})$$

The components of the self-energy of the system of real scalar fields are obtained upon functional differentiation

of the effective action with respect to the components of the correlation function:

$$\Pi^{ij}(x, y) \equiv 2i \frac{\delta \Gamma_2[D, G]}{\delta G^{ji}(y, x)}. \quad (\text{C4})$$

The result of the differentiation reads

$$\Pi_{ij}^{(c)}(x, y) = -\frac{1}{2} g_i g_j^* D^2(x, y) - \frac{1}{2} g_i^* g_j D^2(y, x), \quad (\text{C5a})$$

$$\begin{aligned} \Pi_{ij}^{(d)}(x, y) = & \frac{1}{2} \int_{vu} G^{mn}(v, u) \\ & \times [g_i g_j g_m^* g_n^* D(x, v) D(x, u) D(y, v) D(y, u) \\ & + g_i^* g_j^* g_m g_n D(v, x) D(u, x) D(v, y) D(u, y)]. \end{aligned} \quad (\text{C5b})$$

The next step is to derive the spectral and statistical components of the self-energies (C3) and (C5). Upon use of the decomposition (B14) and of the analogous decomposition of the propagators of the real scalar field, one easily obtains a corresponding decomposition of the self-energies $\Sigma^{(b)}$, $\Sigma^{(c)}$ and $\Pi^{(c)}$ into the statistical and spectral components. Linear combinations of the resulting expressions are presented in Eqs. (11a), (11b), and (12a). The calculation of the spectral and statistical components of $\Sigma^{(d)}$ and $\Pi^{(d)}$, which contain two integrations over space-time, is more involved (see also [39]). Decomposing the two-point correlation functions in Eq. (C3d) into the statistical and spectral components, we get 32 terms. Each of the terms must be integrated over the closed time path \mathcal{C} , see Fig. 10. It is helpful to use relations like the following,

$$\begin{aligned} \int_{\mathcal{C}} du^0 \text{sign}_{\mathcal{C}}(x^0 - u^0) \text{sign}_{\mathcal{C}}(u^0 - y^0) D_\rho(x, u) D_\rho(u, y) \\ = 2 \text{sign}_{\mathcal{C}}(x^0 - y^0) \int_{y^0}^{x^0} du^0 D_\rho(x, u) D_\rho(u, y). \end{aligned} \quad (\text{C6})$$

One then finds that ten terms vanish upon integration over the contour: one term which does not contain any $\text{sign}_{\mathcal{C}}$ functions; five terms which contain only one $\text{sign}_{\mathcal{C}}$ function; two terms which contain a product of two $\text{sign}_{\mathcal{C}}$ functions both depending only on one of the integration variables, u or v ; and finally two terms which contain a product of three $\text{sign}_{\mathcal{C}}$ functions but depend only on one of the “external” arguments, x or y . For the remaining terms integration over the contour \mathcal{C} reduces to a “single time” integration over a combination of the six regions in Fig. 11. Note that the upper limits of the integration never exceed the largest time argument (x^0 in Fig. 11) which ensures the causality of the Kadanoff–Baym equations. In most cases integration over a part of the uv plane can be easily represented as integration over the whole plane, $0 < u, v < \infty$, if two of the spectral functions are replaced by the corresponding retarded and (or) advanced propagators. There are, however, two exceptions: if the resulting integral is only over region (e) or region (f) in Fig. 11. Using the identities

$$\int_{(e)} = \int_{(a+c+e)} + \int_{(b)} - \int_{(a+b+c)}, \quad (\text{C7a})$$

$$\int_{(f)} = \int_{(b+d+f)} + \int_{(a)} - \int_{(a+b+d)}, \quad (\text{C7b})$$

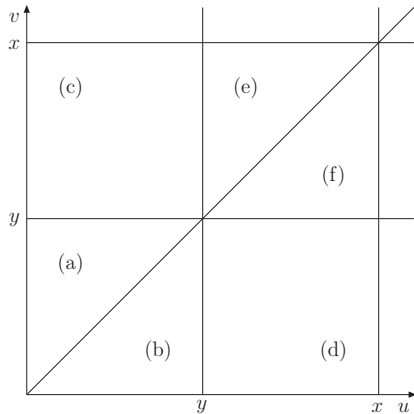


FIG. 11: The integration plane in the case $x^0 > y^0$.

and the definitions of the retarded and advanced propagators, we can represent the corresponding contributions as combinations of integrals over the whole uv plane. Collecting all the terms, we obtain expressions presented in Eqs. (11c) and (12b).

Appendix D: Wigner transformation

To calculate the self-energies entering the Boltzmann equations, we have to Wigner transform products of several two-point functions. Using the definitions (B24), we obtain for the Wigner transform of a product of n functions of the same arguments [30]:

$$f_1(x, y) \dots f_n(x, y) \rightarrow \int d\Pi_{p_1} \dots d\Pi_{p_n} (2\pi)^4 \times \delta^g(p - p_1 - \dots p_n) f(X, p_1) \dots f(X, p_n). \quad (\text{D1})$$

Equation (D1) allows us to Wigner transform the self-energies (11a), (11b) and (12a). The self-energy (11c) has a more complicated structure:

$$f(x, y) = \int_{vu} f_1(y, v) f_2(u, v) f_3(u, x) f_4(y, u) f_5(x, v). \quad (\text{D2})$$

We will now calculate the Wigner transform of (D2) in the Boltzmann approximation. That is, in each f_n we will neglect the deviation of the corresponding center coordinate from $X \equiv X_{xy}$. For instance:

$$f_1(y, v) \rightarrow f_1(X_{yv}, s_{yv}) \rightarrow f_1(X_{xy}, s_{yv}). \quad (\text{D3})$$

In this approximation the integration over u and v induces two conditions on the momenta: $p_v = p_u = 0$, where $p_u = p_2 + p_3 - p_4$ and $p_v = p_1 + p_2 + p_5$. Integration over the relative coordinate s , see Eq. (B24a), induces an additional constraint: $p = p_s$, where $p_s = \frac{1}{2}(p_5 - p_4 - p_3 - p_1)$. Thus, in the Boltzmann approximation the Wigner-transform of (D2) takes the form:

$$f(X, p) = \int d\Pi_{p_1} \dots d\Pi_{p_5} (2\pi)^4 \delta^g(p_u) (2\pi)^4 \delta^g(p_v) \times (2\pi)^4 \delta^g(p - p_s) f_1(X, p_1) \dots f_5(X, p_5) \quad (\text{D4})$$

As far as decays are concerned, two of the momenta in (D4) correspond to the initial and final states, whereas three of the momenta correspond to the internal lines of the loop. The Dirac δ functions in (D4) ensure conservation of four-momentum in each vertex of the loop.

The self-energy (12b) has the structure

$$f(x, y) = \int_{vu} f_1(v, u) f_2(x, v) f_3(x, u) f_4(y, v) f_5(y, u). \quad (\text{D5})$$

Proceeding in the same way, we again obtain (D4) but now with $p_v = p_1 - p_2 - p_4$, $p_u = p_1 + p_3 + p_5$ and $p_s = \frac{1}{2}(p_2 + p_3 - p_4 - p_5)$. This completes the calculation of the Wigner transforms of the self-energies.

Appendix E: Kinematics of the decay

In this appendix, we discuss the kinematics of the decay $\psi_i \rightarrow bb$ in the rest (in the early universe – comoving) frame of the thermal bath and in the rest frame of the decaying heavy particle. For simplicity, we assume that the masses of the toy baryons are negligibly small in comparison with the mass of the heavy real scalar. Let us

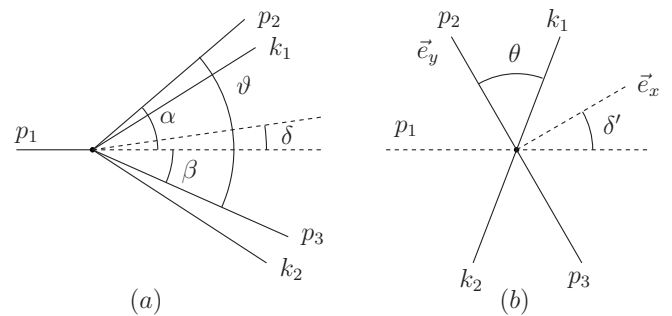


FIG. 12: Decay of the heavy scalar in the rest frame of the plasma and in the rest frame of the decaying particle (see also Fig. 4 for the assignment of the different momenta).

first consider the decay in the rest frame of the thermal bath. Energy-momentum conservation tells us that the momentum p_1 of the decaying particle and the momenta p_2, p_3 of the decay products must lie in the same plane. The latter depend on the scattering angle ϑ , see Fig. 12a. Denoting the angle between the bisectrix of the scattering angle and the momentum \mathbf{p}_1 of the decaying particle by δ we obtain

$$\vartheta = 2 \arccos \left(\frac{|\mathbf{p}_1|}{E_1} \cos \delta \right). \quad (\text{E1})$$

The angles between the momentum of the decaying particle and those of the decay products are given by $\alpha = \vartheta/2 + \delta$ and $\beta = \vartheta/2 - \delta$. If $\delta = 0$ then $\alpha = \beta$. If $\delta \rightarrow \pm \frac{\pi}{2}$, then $\alpha \rightarrow \pi$ and $\beta \rightarrow 0$ and vice versa. Energy-momentum conservation implies, that the energies of the

decay product are related to the angle δ by

$$E_{2,3} = \frac{E_1}{2} \left(1 \mp \frac{|\mathbf{p}_1| \sin \delta}{\sqrt{E_1^2 - |\mathbf{p}_1|^2 \cos^2 \delta}} \right). \quad (\text{E2})$$

If $\mathbf{p}_1 = 0$, then the energy is equally distributed between the decay products. This is also the case if $\mathbf{p}_1 \neq 0$ but $\delta = 0$. In any other case the energy is distributed unequally. In particular if $\delta \rightarrow \frac{\pi}{2}$, then $E_{2,3} = \frac{1}{2}(E_1 \mp |\mathbf{p}_1|)$, so that in the ultrarelativistic limit one of the decay products has almost zero energy, whereas the other receives almost all energy of the decaying particle.

As follows from Eq. (25), to calculate the CP -violating parameter, we need to evaluate the distribution functions associated with the statistical propagators contributing to the vertex loop. As discussed in Sec. III, only those two terms of (25) for which both intermediate toy baryons are on-shell, whereas the real scalar is off-shell, contribute to the CP -violating parameter (see Fig. 4a). Since both momenta k_1 and k_2 of the internal toy baryon lines are on-shell, the kinematics of these intermediate states is the same as the kinematics of the decay products. However, due to the presence of the intermediate off-shell real scalar, the corresponding scattering angle does not need to be equal to ϑ and the angle between the two scattering planes can differ from zero. It is somewhat easier to perform the simultaneous analysis of the intermediate and final states' kinematics in the rest frame of the decaying particle. The Lorentz transformation between the two frames reads

$$\hat{\Lambda} = \frac{1}{M} \begin{pmatrix} E_1 & -|\mathbf{p}_1| \\ -|\mathbf{p}_1| & E_1 \end{pmatrix}. \quad (\text{E3})$$

As follows from Eq. (E1), in the new frame the scattering angle is $\vartheta' = \pi$ for both intermediate and final states, whereas Eq. (E2) implies that the energies are equal to $M/2$. Using the fact that components of the momentum orthogonal to the direction of the boost are invariant under transformation (E3), we can calculate the angle δ in the new frame:

$$\sin \delta' = \frac{E_1 \sin \delta}{\sqrt{E_1^2 - |\mathbf{p}_1|^2 \cos^2 \delta}} = (|\mathbf{p}_3| - |\mathbf{p}_2|)/|\mathbf{p}_1|. \quad (\text{E4})$$

It then follows that $\delta' > \delta$ since the denominator of (E4) is smaller than E_1 .

For a homogeneous and isotropic system the one-particle distribution functions depend only on the Lorentz-invariant product ku , where k is the particles' momentum and u is the four-velocity of the thermal bath's rest frame with respect to the chosen frame of reference. In particular in thermal equilibrium:

$$f^{eq}(k) = [\exp((ku - \mu)/T) - 1]^{-1}. \quad (\text{E5})$$

In the rest frame of the gas $u = (1, 0, 0, 0)$, and we recover the usual Bose–Einstein distribution. Applying the

Lorentz transformations (E3), we can deduce u in the rest frame of the decaying particle

$$u = M^{-1}(E_1, -\mathbf{p}_1). \quad (\text{E6})$$

Introducing an orthogonal coordinate system, as is depicted in Fig. 12, we can then express the arguments of the distribution functions in the form:

$$uk_{1,2} = \frac{1}{2}[E_1 + |\mathbf{p}_1|(\sin \theta \cos \varphi \cos \delta' \mp \cos \theta \sin \delta')], \quad (\text{E7})$$

where φ is the angle between the scattering planes of the intermediate and final states (not depicted in Fig. 12).

Appendix F: Thermal average of the CP -violating parameter

The CP -violating parameter in vacuum is momentum-independent due to Lorentz invariance. Since the surrounding medium defines a preferred frame (its rest frame), the effective CP -violating parameter in medium depends explicitly on the momenta of the participating particles (see Fig. 4). In order to investigate the order of magnitude of the medium corrections, we consider the thermally averaged CP -violating parameter:

$$\langle \epsilon_i \rangle = \frac{\int d\Pi_{p_1}^3 d\Pi_{p_2}^3 d\Pi_{p_3}^3 w(p_1, p_2, p_3) \epsilon_i(p_1, p_2)}{\int d\Pi_{p_1}^3 d\Pi_{p_2}^3 d\Pi_{p_3}^3 w(p_1, p_2, p_3)}, \quad (\text{F1})$$

where $\epsilon_i(p_1, p_2) = \epsilon_i^{vac} + \delta \epsilon_i^{med}(p_1, p_2)$ and w represents the gain or loss term (they are equal in equilibrium). For the decay processes:

$$w(p_1, p_2, p_3) = (2\pi)^4 \delta(E_1 - E_2 - E_3) \delta(\mathbf{p}_1 - \mathbf{p}_2 - \mathbf{p}_3) \times f(\mathbf{p}_2) \bar{f}(\mathbf{p}_3) [1 + f_{\psi_i}(\mathbf{p}_1)]. \quad (\text{F2})$$

In the hierarchical limit $M_1 \ll M_2$, the CP -violating parameter ϵ_1 only depends on $|\mathbf{p}_1|$, see Eq. (31). Furthermore, we set $m \rightarrow 0$ here. Integrating in (F1) over momenta of the final states, we find in this approximation:

$$\langle \epsilon_1 \rangle = \frac{\int_0^\infty dq \omega(q) \epsilon_1(q)}{\int_0^\infty dq \omega(q)},$$

where $q = |\mathbf{p}_1|$. To calculate the weighting function $\omega(q)$ we insert thermal distributions characterized by a common temperature T and zero chemical potential. We consider two cases:

- (i) in the first case we insert Bose–Einstein (BE) distributions for f and f_{ψ_i} in (F2);
- (ii) in the second case we insert Maxwell–Boltzmann (MB) distribution for f and neglect f_{ψ_i} in (F2).

The resulting expressions for the weighting function read:

$$w(q) = \begin{cases} \frac{2q}{E_q \sinh^2\left(\frac{E_q}{2T}\right)} \ln \left(\frac{\sinh\left(\frac{E_q+q}{4T}\right)}{\sinh\left(\frac{E_q-q}{4T}\right)} \right) & \text{BE} , \\ q^2 \exp\left(-\frac{E_q}{T}\right) & \text{MB} , \end{cases} \quad (\text{F3})$$

where $E_q = \sqrt{M_1^2 + q^2}$.

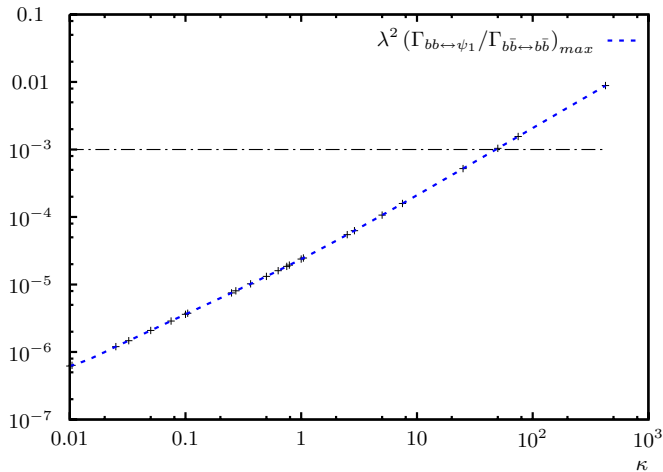


FIG. 13: The maximum value of the ratio of the rates for $bb \leftrightarrow \psi$ and $b\bar{b} \leftrightarrow b\bar{\psi}$ over washout factor κ .

Appendix G: Numerical details

To solve the system of Boltzmann equations (36), we introduce the transformed variables $x = a(t)$ and $k_i = Sa(t)|\mathbf{p}_i|$ for time and momentum. The constant factor S is chosen such that $Sx = T^{-1} = (2 \cdot 1.66 \sqrt{g_*}/M_{\text{Pl}}t)^{\frac{1}{2}}$. The distributions as functions of the transformed momenta are then well represented, in some sense, in the range $k_i \simeq 0.025 - 50.0$.¹⁷ In addition, we introduce the transformed on-shell energies and masses, $m_i = SxM_i$ and $k_i^0 = (k_i^2 + m_i^2)^{\frac{1}{2}} = Sx(|\mathbf{p}_i|^2 + M_i^2)^{\frac{1}{2}}$. In these coordinates the Liouville operator for Robertson–Walker space-time takes the form $L[f](|\mathbf{p}|) \rightarrow S^{-1}Hk_1^0 \partial \tilde{f}(k_1)/\partial x$, where $\tilde{f}(k_1)$ is the transformed one-particle distribution function dependent on k_1 and x . Defining $\tilde{L}[\tilde{f}](k_1) \equiv \partial \tilde{f}(k_1)/\partial x$, the Boltzmann equations can be written in the form $\tilde{L}[\tilde{f}](k_1) = \tilde{C}[\tilde{f}](k_1)$ with transformed collision integral $\tilde{C}[\tilde{f}]$.

Homogeneity and isotropy can be exploited to simplify the collision integrals significantly. In [76], it has been shown how the various collision terms for decays, inverse decays and 2 – 2 scattering can be reduced to lower dimensional integrals in general. Here, we transform the integrals to the new coordinates at the same time. In particular, the collision integrals for a scattering process $12 \leftrightarrow 34$ (here $b\bar{b} \leftrightarrow b\bar{\psi}$, $b\bar{b} \leftrightarrow b\bar{b}$ and $b\bar{b} \leftrightarrow b\bar{\psi}$) can be

¹⁷ In particular we require that the approximate numerical value of the moments (G7) are close to their true values for close-to-equilibrium distributions. Also we demand that particles created in decays are not produced with momenta outside of this range to a significant extent so that total number densities show the expected behavior.

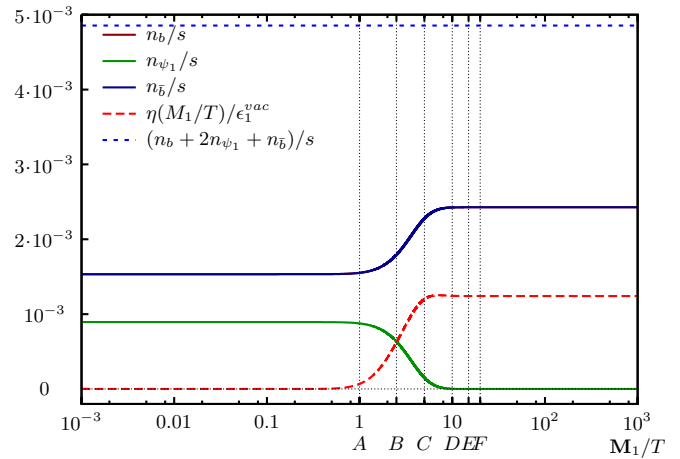


FIG. 14: Number densities of the various species and the generated asymmetry η as functions of M_1/T for $\kappa \simeq 0.366$ (case c). The total number density is approximately conserved.

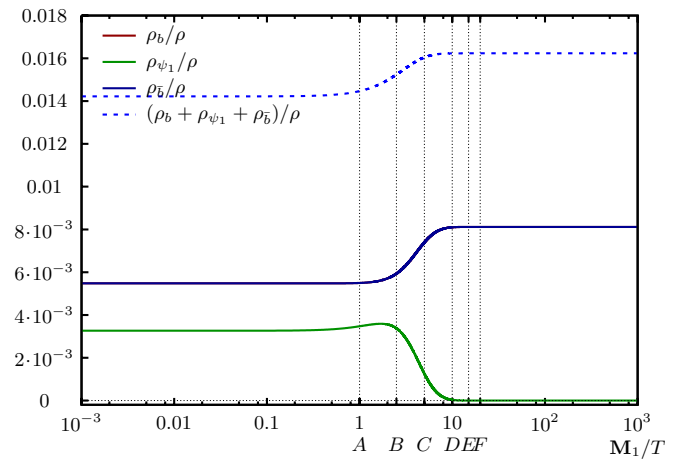


FIG. 15: Energy densities of the various species as functions of M_1/T for $\kappa \simeq 0.366$ (case c). The ratio of the total energy density $\rho_b + \rho_{\bar{b}} + \rho_{\psi}$ and the total cosmological energy density ρ is not constant. This feature is due to the different scaling behavior of relativistic and nonrelativistic species. For this reason the ratio ρ_{ψ}/ρ increases slightly before the particles start to decay. This is more pronounced for smaller washout factors (see Fig. 19).

reduced to a twofold integral:

$$\begin{aligned} \tilde{C}_{12 \leftrightarrow 34}[\tilde{f}_1 \cdot](k_1) = & \frac{1}{SHx^2} \frac{1}{64\pi^3 k_1^0} \int \int \frac{k_3 dk_3}{k_3^0} \frac{k_4 dk_4}{k_4^0} \theta(k_2^0 - m_2) D_{12 \leftrightarrow 34} \times \\ & \{ [1 + \tilde{f}_1(k_1)] [1 + \tilde{f}_2(k_2)] \tilde{f}_3(k_3) \tilde{f}_4(k_4) - \\ & \tilde{f}_1(k_1) \tilde{f}_2(k_2) [1 + \tilde{f}_3(k_3)] [1 + \tilde{f}_4(k_4)] \}, \end{aligned} \quad (\text{G1})$$

where $k_2^0 = k_3^0 + k_4^0 - k_1^0$ and $k_2 = [(k_2^0)^2 - m_2^2]^{\frac{1}{2}}$. The integrated scattering kernel $D_{12 \leftrightarrow 34}$ for a constant (momentum-independent) amplitude \mathcal{A} and for massless

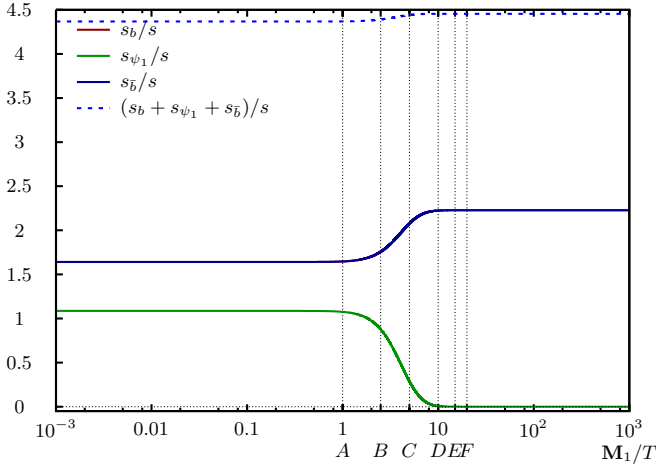


FIG. 16: Entropy densities of the various species and the total entropy density $(s_b + s_{\bar{b}} + s_{\psi})/s$ as functions of M_1/T for $\kappa \simeq 0.366$ (case c).

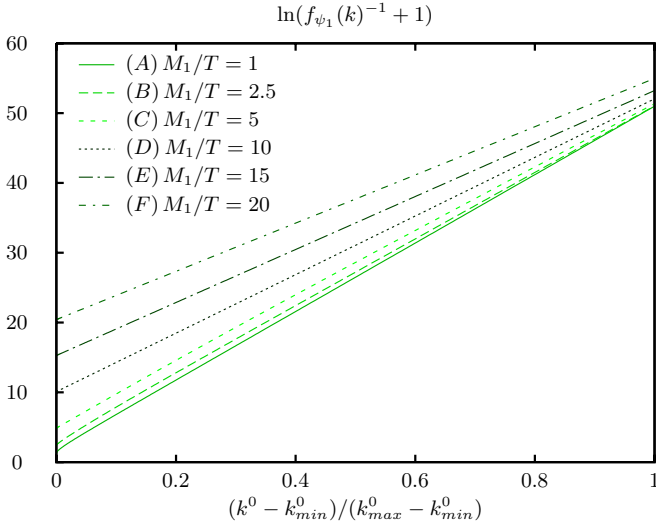


FIG. 17: Deviation of the distribution function f_{ψ_1} from equilibrium for washout factor $\kappa \simeq 0.366$ (case c).

species 1, 2, 3 and 4 is given by

$$D_{12 \leftrightarrow 34}(k_1, k_2, k_3, k_4) = \frac{\mathcal{A}}{2k_1} \theta(k_3 + k_4 - |k_1 - k_2|) \times \theta(k_1 + k_2 - |k_3 - k_4|) (k_3 + k_4 - |k_3 - k_1| - |k_4 - k_1|). \quad (\text{G2})$$

Similarly, the collision integrals for a particle created in inverse decays, $1 \leftrightarrow 23$ (here $\psi_1 \leftrightarrow b\bar{b}$ and $\psi_1 \leftrightarrow \bar{b}b$), can be reduced to a single integral:

$$\tilde{C}_{1 \leftrightarrow 23}[\tilde{f}_1](k_1) = \frac{S}{H} \frac{1}{32\pi k_1^0} \int \frac{k_3 dk_3}{k_3^0} \theta(k_2^0 - m_2) D_{1 \leftrightarrow 23} \times \{ [1 + \tilde{f}_1(k_1)] \tilde{f}_2(k_2) \tilde{f}_3(k_3) - \tilde{f}_1(k_1) [1 + \tilde{f}_2(k_2)] [1 + \tilde{f}_3(k_3)] \}, \quad (\text{G3})$$

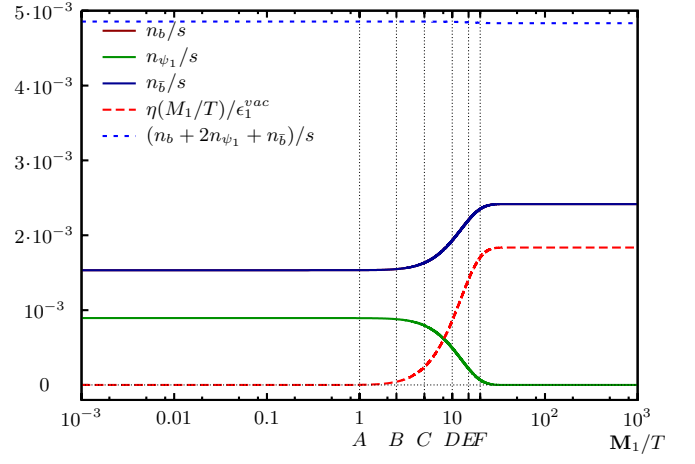


FIG. 18: Number densities of the various species and the generated asymmetry η as functions of M_1/T for $\kappa \simeq 0.01$ (case a).

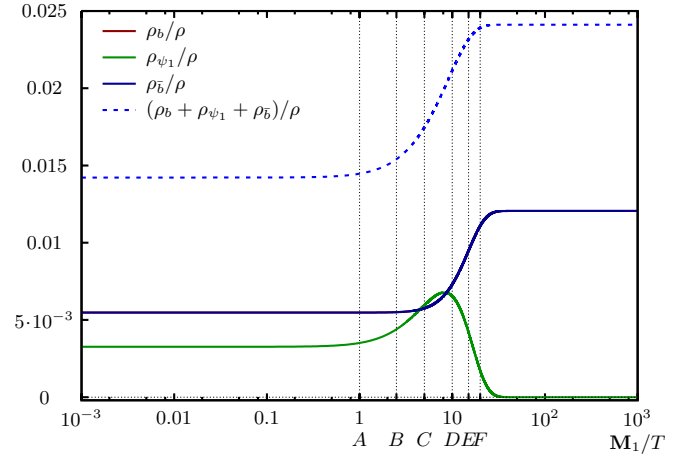


FIG. 19: Energy densities of the various species and the total energy density $(\rho_b + \rho_{\bar{b}} + \rho_{\psi})/\rho$ as functions of M_1/T for $\kappa \simeq 0.01$ (case a).

where $k_2^0 = k_1^0 - k_3^0$ and $k_2 = [(k_2^0)^2 - m_2^2]^{\frac{1}{2}}$. The integrated scattering kernel $D_{1 \leftrightarrow 23}$ is given by

$$D_{1 \leftrightarrow 23}(k_1, k_2, k_3) = \frac{2\mathcal{A}}{k_1} \theta(k_1 - |k_2 - k_3|) \theta((k_2 + k_3) - k_1). \quad (\text{G4})$$

Finally, the collision integrals for a particle created in decays, $12 \leftrightarrow 3$ (here $b\bar{b} \leftrightarrow \psi_1$ and $\bar{b}b \leftrightarrow \psi_1$), can be reduced to the single integral

$$\tilde{C}_{12 \leftrightarrow 3}[\tilde{f}_1](k_1) = \frac{S}{H} \frac{1}{32\pi k_1^0} \int \frac{k_3 dk_3}{k_3^0} \theta(k_2^0 - m_2) D_{12 \leftrightarrow 3} \times \{ [1 + \tilde{f}_1(k_1)] [1 + \tilde{f}_2(k_2)] \tilde{f}_3(k_3) - \tilde{f}_1(k_1) \tilde{f}_2(k_2) [1 + \tilde{f}_3(k_3)] \}, \quad (\text{G5})$$

where $k_2^0 = k_3^0 - k_1^0$ and $k_2 = [(k_2^0)^2 - m_2^2]^{\frac{1}{2}}$. The inte-

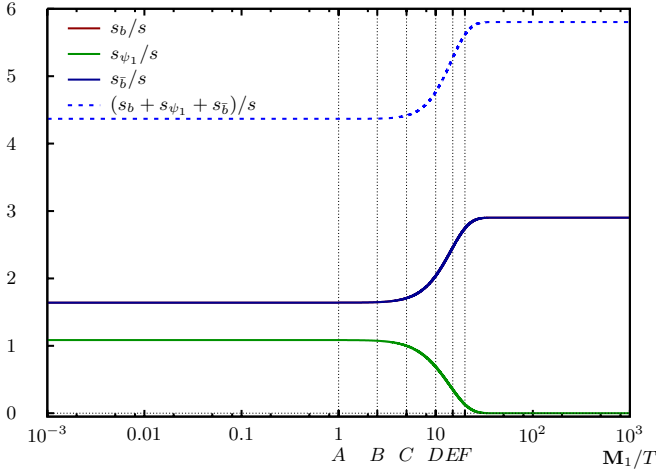


FIG. 20: Entropy densities of the various species and the total entropy density $(s_b + s_{\bar{b}} + s_{\psi})/s$ as functions of M_1/T for $\kappa \simeq 0.01$ (case a).

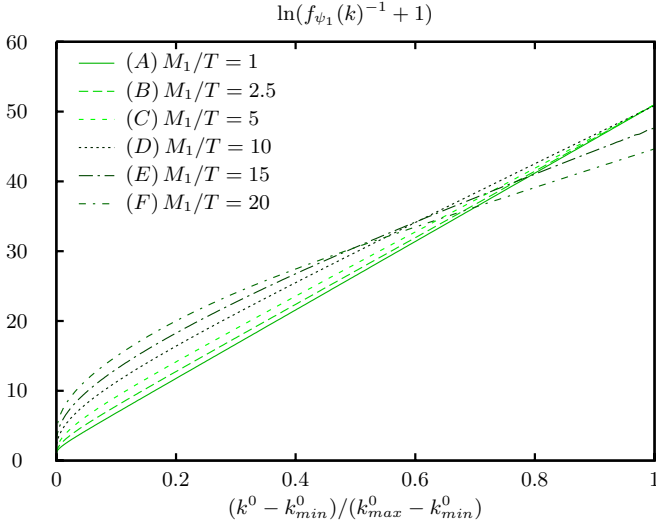


FIG. 21: Deviation of the distribution function f_{ψ_1} from equilibrium for washout factor $\kappa \simeq 0.01$ (case a).

grated scattering kernel $D_{12\leftrightarrow 3}$ is given by

$$D_{12\leftrightarrow 3}(k_1, k_2, k_3) = \frac{2\mathcal{A}}{k_1} \theta(k_3 - |k_1 - k_2|) \theta((k_1 + k_2) - k_3). \quad (\text{G6})$$

Number density and energy density corresponding to the distribution \tilde{f} in transformed coordinates read

$$n[\tilde{f}] = \frac{1}{2\pi^2} \left(\frac{1}{S_x}\right)^3 \int (k_1)^2 \tilde{f}(k_1) dk_1, \\ \rho[\tilde{f}] = \frac{1}{2\pi^2} \left(\frac{1}{S_x}\right)^4 \int (k_1)^2 k_1^0 \tilde{f}(k_1) dk_1. \quad (\text{G7})$$

For massless particles these are the second and third moment of the distribution, respectively. As outlined in

Sec. IV, we assume that the interactions $bb \leftrightarrow bb$, $\bar{b}\bar{b} \leftrightarrow \bar{b}\bar{b}$ and $b\bar{b} \leftrightarrow b\bar{b}$ are rapid enough to keep the distribution functions of b and \bar{b} very close to their equilibrium distributions, parametrized by a_0, a_1, \bar{a}_0 and \bar{a}_1 :

$$f_a^{eq}(k_1) = [\exp(a_0 + a_1 k_1) - 1]^{-1}, \\ \bar{f}_a^{eq}(k_1) = [\exp(\bar{a}_0 + \bar{a}_1 k_1) - 1]^{-1}. \quad (\text{G8})$$

Assuming that $b\bar{b} \leftrightarrow b\bar{b}$ alone is much faster than the inverse decays into ψ_1 , the evolution of f and \bar{f} can therefore be described by means of three parameters a_0, \bar{a}_0 and a_1 . The equations for the evolution of these parameters are obtained by forming the moments $n[\cdot]$ of Eqs. (36a) and (36b):¹⁸

$$n[\tilde{L}[f_a^{eq}]] = \frac{da_0}{dx} n\left[\frac{\partial f_a^{eq}}{\partial a_0}\right] + \frac{da_1}{dx} n\left[\frac{\partial f_a^{eq}}{\partial a_1}\right] = n[\tilde{C}_{bb\leftrightarrow\psi_1}], \\ n[\tilde{L}[\bar{f}_a^{eq}]] = \frac{d\bar{a}_0}{dx} n\left[\frac{\partial \bar{f}_a^{eq}}{\partial \bar{a}_0}\right] + \frac{d\bar{a}_1}{dx} n\left[\frac{\partial \bar{f}_a^{eq}}{\partial \bar{a}_1}\right] = n[\tilde{C}_{\bar{b}\bar{b}\leftrightarrow\psi_1}]. \quad (\text{G9})$$

Here, we used $n[\tilde{C}_{bb\leftrightarrow bb}[f]] = n[\tilde{C}_{\bar{b}\bar{b}\leftrightarrow\bar{b}\bar{b}}[\bar{f}]] = 0$ and $n[\tilde{C}_{b\bar{b}\leftrightarrow b\bar{b}}[f, \bar{f}]] = n[\tilde{C}_{\bar{b}b\leftrightarrow\bar{b}b}[\bar{f}, f]] = 0$. The third equation is obtained by forming the moment $\rho[\cdot]$ of the sum of Eqs. (36a) and (36b), i.e.

$$\rho[\tilde{L}[f_a^{eq}]] + \rho[\tilde{L}[\bar{f}_a^{eq}]] = \frac{da_0}{dx} \rho\left[\frac{\partial f_a^{eq}}{\partial a_0}\right] + \frac{d\bar{a}_0}{dx} \rho\left[\frac{\partial \bar{f}_a^{eq}}{\partial \bar{a}_0}\right] + \frac{da_1}{dx} \rho\left[\frac{\partial f_a^{eq}}{\partial a_1}\right] + \frac{d\bar{a}_1}{dx} \rho\left[\frac{\partial \bar{f}_a^{eq}}{\partial \bar{a}_1}\right] = \rho[\tilde{C}_{bb\leftrightarrow\psi_1}] + \rho[\tilde{C}_{\bar{b}\bar{b}\leftrightarrow\psi_1}], \quad (\text{G10})$$

where we used $\rho[\tilde{C}_{b\bar{b}\leftrightarrow b\bar{b}}[f, \bar{f}]] + \rho[\tilde{C}_{\bar{b}b\leftrightarrow\bar{b}b}[\bar{f}, f]] = 0$. The derivatives of f_a^{eq} with respect to the parameters a_i can be rewritten as

$$\frac{\partial f_a^{eq}(k_1)}{\partial a_i} = -(k_1^0)^i [1 + f_a^{eq}(k_1)] f_a^{eq}(k_1), \quad i = 0, 1. \quad (\text{G11})$$

An analogous relation holds for the derivatives of \bar{f}_a^{eq} with respect to \bar{a}_0 and \bar{a}_1 . Solving Eqs. (G9) and (G10) for da_0/dx , $d\bar{a}_0/dx$ and da_1/dx , we find the differential

¹⁸ Here and in the following we use the abbreviations $\tilde{C}_{bb\leftrightarrow\psi_1} = \tilde{C}_{bb\leftrightarrow\psi_1}[f_a^{eq}, f_{\psi_1}]$ and $\tilde{C}_{\bar{b}\bar{b}\leftrightarrow\psi_1} = \tilde{C}_{\bar{b}\bar{b}\leftrightarrow\psi_1}[\bar{f}_a^{eq}, f_{\psi_1}]$. Also note that f, \bar{f} and f_{ψ_1} are functions of the transformed coordinates, here.

equations for the three parameters:

$$\begin{aligned}
\frac{da_0}{dx} &= -\frac{\dot{a}_1 n [k_1^0 (1 + f_a^{eq}) f_a^{eq}] + n [\tilde{C}_{bb \leftrightarrow \psi_1}]}{n [(1 + f_a^{eq}) f_a^{eq}]}, \\
\frac{d\bar{a}_0}{dx} &= -\frac{\dot{a}_1 n [k_1^0 (1 + \bar{f}_a^{eq}) \bar{f}_a^{eq}] + n [\tilde{C}_{\bar{b}\bar{b} \leftrightarrow \psi_1}]}{n [(1 + \bar{f}_a^{eq}) \bar{f}_a^{eq}]}, \\
\frac{da_1}{dx} &= -\left((n [\tilde{C}_{bb \leftrightarrow \psi_1}] \rho_f + n [k_1^0 (1 + f_a^{eq}) f_a^{eq}] \rho_C) \right. \\
&\quad \times n [(1 + \bar{f}_a^{eq}) \bar{f}_a^{eq}] \rho [(1 + f_a^{eq}) f_a^{eq}] \\
&\quad + (n [\tilde{C}_{\bar{b}\bar{b} \leftrightarrow \psi_1}] \rho_f + n [k_1^0 (1 + \bar{f}_a^{eq}) \bar{f}_a^{eq}] \rho_C) \\
&\quad \times n [(1 + f_a^{eq}) f_a^{eq}] \rho [(1 + \bar{f}_a^{eq}) \bar{f}_a^{eq}] \Big) / h + \rho_C / \rho_f, \quad (G12)
\end{aligned}$$

where we have defined

$$\begin{aligned}
h &= \rho_f \left(n [(1 + f_a^{eq}) f_a^{eq}] n [(1 + \bar{f}_a^{eq}) \bar{f}_a^{eq}] \rho_f \right. \\
&\quad + n [k_1^0 (1 + \bar{f}_a^{eq}) \bar{f}_a^{eq}] n [(1 + f_a^{eq}) f_a^{eq}] \rho [(1 + \bar{f}_a^{eq}) \bar{f}_a^{eq}] \\
&\quad \left. + n [k_1^0 (1 + f_a^{eq}) f_a^{eq}] n [(1 + \bar{f}_a^{eq}) \bar{f}_a^{eq}] \rho [(1 + f_a^{eq}) f_a^{eq}] \right), \quad (G13)
\end{aligned}$$

as well as

$$\begin{aligned}
\rho_f &= -\rho [k_1^0 (1 + f_a^{eq}) f_a^{eq}] - \rho [k_1^0 (1 + \bar{f}_a^{eq}) \bar{f}_a^{eq}], \\
\rho_C &= \rho [\tilde{C}_{bb \leftrightarrow \psi_1}] + \rho [\tilde{C}_{\bar{b}\bar{b} \leftrightarrow \psi_1}]. \quad (G14)
\end{aligned}$$

As stated in the main text, we need to start with finite chemical potentials as to avoid the occurrence of Bose-Einstein condensation. We choose the minimal acceptable value $a_0 = \bar{a}_0 = 0.5$, corresponding to $\mu_b = \mu_{\bar{b}} = -0.5 T_0$ and $\mu_{\psi_1} = 2\mu_b$. The initial value $a_1 = 1$ corresponds to the initial cosmological temperature T_0 . We checked that the results do not depend on T_0 as long as $T_0 \gg M_1$. The heavy species ψ_1 is subject to relatively weak interactions only, so that its distribution function can deviate from kinetic equilibrium. Therefore, we solve the full Boltzmann equation for ψ_1 ,

$$\tilde{L}[f_{\psi_1}](k_1) = \tilde{C}_{\psi_1 \leftrightarrow bb} [f_{\psi_1}, f](k_1) + \tilde{C}_{\psi_1 \leftrightarrow \bar{b}\bar{b}} [f_{\psi_1}, \bar{f}](k_1), \quad (G15)$$

along with the integrated ones for b and \bar{b} .

Because of the integration of the equations for the massless species all collision terms for $2-2$ scattering drop out of the system. In order to verify that the rates for these processes are much larger than the ones of the decays and inverse decays we have computed the rates for these processes numerically. The maximum (during the full evolution) of the ratio of $\Gamma_{bb \leftrightarrow \psi_1}$ and $\Gamma_{\bar{b}\bar{b} \leftrightarrow b\bar{b}}$ is exemplarily presented in Fig. 13 (the rates for the other

$2-2$ processes are similar). It shows that we can choose $\lambda \sim 1$ or smaller for most of the relevant range of $|g|^2$ if we demand that $\Gamma_{\bar{b}\bar{b} \leftrightarrow b\bar{b}} / \Gamma_{bb \leftrightarrow \psi_1} \gtrsim 10^3$ as criterion that b and \bar{b} are in kinetic equilibrium at all times. Here the equilibrium shape of f and \bar{f} is not distorted by the expansion since we are dealing with massless particles. In addition, it can be argued that the $2-2$ processes are meant to model rapid gauge interactions with different particles which would have the same effect of equilibrating b and \bar{b} . In this sense we could even formally tolerate nonperturbative values of λ .

To turn the equations into a system of ordinary differential equations (ODE) the distribution functions were discretized on a grid of dimension 400 with linearly increasing spacings in the range $k_1 \simeq 0.025 \dots 50.0$ to account for the characteristic behavior of close-to-equilibrium distributions at small and large momenta. All integrals were approximated by Riemann sums on this grid. The system of Boltzmann equations behaves numerically stiff. This means that it is advisable to use an implicit method for its numerical solution to achieve acceptable step sizes (and hence acceptable execution times and numerical errors). Here CVODE with its backward differentiation formula with Newton iteration was used as ODE solver. The full Jacobian was computed analytically in every external step. A relative tolerance of 10^{-8} was attributed to every momentum mode. Because of the implicit method all solutions were computed in $\mathcal{O}(10^3)$ steps.

Since the global systematic error due to the discretization cannot be computed within the method the proper behavior of the system was tested by successive refinement of the grid and comparison of some of the macroscopic quantities with the theory predictions. For this purpose, we present two examples of the number densities n_x , the energy densities ρ_x and the entropy densities for the washout factors $\kappa \simeq 0.366$ (case c in Fig. 14-16) and $\kappa \simeq 0.01$ (case a in Fig. 18-20). The total number density $(n_b + 2n_{\psi_1} + n_{\bar{b}})/s$ is almost conserved (as discussed in Sec. IV). The ratio $(\rho_b + \rho_{\psi_1} + \rho_{\bar{b}})/\rho$ is not constant (see Fig. 15). This behavior is expected for a system involving nonrelativistic massive particles and is also observed for the bottom-up equations. The ratio is much smaller than one so that it is justified to neglect the backreaction on the curvature. Finally, the total entropy density is steadily increasing as it should. Figures 17 and 21 show the deviation of the distribution function f_{ψ_1} from kinetic equilibrium ones for which the curves would be straight lines. The deviation from equilibrium is larger for smaller values of κ and increases at late times, as expected.

[1] E. W. Kolb and M. S. Turner, *The Early universe* (1990), redwood City, CA: Addison-Wesley 547 p. (Frontiers in

physics, 69).

[2] G. Hinshaw et al. (WMAP), *Astrophys. J. Suppl.* **180**,

- 225 (2009), 0803.0732.
- [3] E. Komatsu et al. (WMAP), *Astrophys. J. Suppl.* **180**, 330 (2009), 0803.0547.
 - [4] A. D. Sakharov, *JETP Letters* **5**, 24 (1967).
 - [5] G. 't Hooft, *Phys. Rev. Lett.* **37**, 8 (1976).
 - [6] V. A. Kuzmin, V. A. Rubakov, and M. E. Shaposhnikov, *Phys. Lett. B* **155**, 36 (1985).
 - [7] M. Fukugita and T. Yanagida, *Phys. Lett. B* **174**, 45 (1986).
 - [8] E. Nardi, Y. Nir, E. Roulet, and J. Racker, *JHEP* **01**, 164 (2006), hep-ph/0601084.
 - [9] A. Abada, S. Davidson, F.-X. Josse-Michaux, M. Losada, and A. Riotto, *JCAP* **0604**, 004 (2006), hep-ph/0601083.
 - [10] A. Abada et al., *JHEP* **09**, 010 (2006), hep-ph/0605281.
 - [11] R. Barbieri, P. Creminelli, A. Strumia, and N. Tetradis, *Nucl. Phys. B* **575**, 6177 (2000), hep-ph/9911315.
 - [12] S. Blanchet and P. Di Bari, *JCAP* **0703**, 018 (2007), hep-ph/0607330.
 - [13] S. Blanchet and P. Di Bari, *Nucl. Phys. Proc. Suppl.* **168**, 372 (2007), hep-ph/0702089.
 - [14] A. Anisimov, S. Blanchet, and P. Di Bari, *JCAP* **0804**, 033 (2008), 0707.3024.
 - [15] S. Antusch and A. M. Teixeira, *JCAP* **0702**, 024 (2007), hep-ph/0611232.
 - [16] S. Antusch, S. F. King, and A. Riotto, *JCAP* **0611**, 011 (2006), hep-ph/0609038.
 - [17] A. Pilaftsis and T. E. J. Underwood, *Nucl. Phys. B* **692**, 303345 (2004), hep-ph/0309342.
 - [18] A. Pilaftsis and T. E. J. Underwood, *Phys. Rev. D* **72**, 113001 (2005), hep-ph/0506107.
 - [19] L. Covi, N. Rius, E. Roulet, and F. Vissani, *Phys. Rev. D* **57**, 9399 (1998), hep-ph/9704366.
 - [20] G. F. Giudice, A. Notari, M. Raidal, A. Riotto, and A. Strumia, *Nucl. Phys. B* **685**, 89149 (2004), hep-ph/0310123.
 - [21] W. Buchmüller and S. Fredenhagen, *Phys. Lett. B* **483**, 217224 (2000), hep-ph/0004145.
 - [22] A. De Simone and A. Riotto, *JCAP* **0708**, 002 (2007), hep-ph/0703175.
 - [23] A. De Simone and A. Riotto, *JCAP* **0708**, 013 (2007), 0705.2183.
 - [24] A. De Simone (2008), 0805.2354.
 - [25] A. Anisimov, W. Buchmüller, M. Drewes, and S. Mendizabal, *Annals Phys.* **324**, 12341260 (2009), 0812.1934.
 - [26] M. Flanz, E. A. Paschos, and U. Sarkar, *Phys. Lett. B* **345**, 248252 (1995), erratum-ibid.B382:447,1996, hep-ph/9411366.
 - [27] L. Covi, E. Roulet, and F. Vissani, *Phys. Lett. B* **384**, 169174 (1996), hep-ph/9605319.
 - [28] A. Pilaftsis, *Phys. Rev. D* **56**, 5431 (1997).
 - [29] M. Garny, A. Hohenegger, A. Kartavtsev, and M. Lindner (2009), 0911.4122.
 - [30] A. Hohenegger, A. Kartavtsev, and M. Lindner, *Phys. Rev. D* **78**, 085027 (2008), 0807.4551.
 - [31] P. Danielewicz, *Annals Phys.* **152**, 239 (1984).
 - [32] Y. B. Ivanov, J. Knoll, and D. N. Voskresensky, *Nucl. Phys. A* **672**, 313356 (2000), nucl-th/9905028.
 - [33] J. Knoll, Y. B. Ivanov, and D. N. Voskresensky, *Annals Phys.* **293**, 126 (2001), nucl-th/0102044.
 - [34] J.-P. Blaizot and E. Iancu, *Phys. Rept.* **359**, 355 (2002), hep-ph/0101103.
 - [35] A. Tranberg, *JHEP* **11**, 037 (2008), 0806.3158.
 - [36] J.-P. Blaizot, E. Iancu, and U. Reinosa, *Nucl. Phys. A* **736**, 149200 (2004), hep-ph/0312085.
 - [37] G. Aarts and J. Berges, *Phys. Rev. D* **64**, 105010 (2001), hep-ph/0103049.
 - [38] J. Berges, *AIP Conf. Proc.* **739**, 362 (2004), hep-ph/0409233.
 - [39] M. E. Carrington and S. Mrowczynski, *Phys. Rev. D* **71**, 065007 (2005), hep-ph/0406097.
 - [40] P. Danielewicz, *Annals Phys.* **152**, 305 (1984).
 - [41] J. Berges and J. Cox, *Phys. Lett. B* **517**, 369374 (2001), hep-ph/0006160.
 - [42] J. Berges, *Nucl. Phys. A* **699**, 847886 (2002), hep-ph/0105311.
 - [43] G. Aarts and J. Berges, *Phys. Rev. Lett.* **88**, 041603 (2002), hep-ph/0107129.
 - [44] J. Berges, S. Borsanyi, and J. Serreau, *Nucl. Phys. B* **660**, 5180 (2003), hep-ph/0212404.
 - [45] S. Juchem, W. Cassing, and C. Greiner, *Phys. Rev. D* **69**, 025006 (2004), hep-ph/0307353.
 - [46] A. Arrizabalaga, J. Smit, and A. Tranberg, *Phys. Rev. D* **72**, 025014 (2005), hep-ph/0503287.
 - [47] M. Lindner and M. M. Mller, *Phys. Rev. D* **73**, 125002 (2006), hep-ph/0512147.
 - [48] M. Lindner and M. M. Mller, *Phys. Rev. D* **77**, 025027 (2008), 0710.2917.
 - [49] S. Weinstock, *Phys. Rev. D* **73**, 025005 (2006), hep-ph/0510417.
 - [50] F. Fillion-Gourdeau, J.-S. Gagnon, and S. Jeon, *Phys. Rev. D* **74**, 025010 (2006), hep-ph/0603212.
 - [51] J. Winter, *Phys. Rev. D* **32**, 1871 (1985).
 - [52] M. L. Bellac, *Thermal Field Theory* (Cambridge University Press, Cambridge, 2000), ISBN 0-521-65477-7.
 - [53] N. P. Landsman and C. G. van Weert, *Phys. Rept.* **145**, 141 (1987).
 - [54] Y. B. Ivanov, J. Knoll, and D. N. Voskresensky, *Nucl. Phys. A* **657**, 413445 (1999), hep-ph/9807351.
 - [55] M. Garny, A. Hohenegger, A. Kartavtsev, and M. Lindner (2009), in preparation.
 - [56] F. Hahn-Woernle, M. Plmacher, and Y. Y. Y. Wong, *JCAP* **0908**, 028 (2009), 0907.0205.
 - [57] A. Basbll and S. Hannestad, *JCAP* **0701**, 003 (2007), hep-ph/0609025.
 - [58] J. Garayoa, S. Pastor, T. Pinto, N. Rius, and O. Vives, *JCAP* **0909**, 035 (2009), 0905.4834.
 - [59] G. 't Hooft and M. Veltman, *Nucl. Phys. B* **153**, 365 (1979).
 - [60] G. J. van Oldenborgh and J. A. M. Vermaseren, *Zeitschrift fr Physik C Particles and Fields* **46**, 425 (1990).
 - [61] J. M. Cornwall, R. Jackiw, and E. Tomboulis, *Phys. Rev. D* **10**, 2428 (1974).
 - [62] J. S. Schwinger, *J. Math. Phys.* **2**, 407 (1961).
 - [63] L. V. Keldysh, *Zh. Eksp. Teor. Fiz.* **47**, 1515 (1964).
 - [64] P. M. Bakshi and K. T. Mahanthappa, *Journal of Mathematical Physics* **4**, 1 (1963).
 - [65] K. Chou, Z. Su, B. Hao, and L. Yu, *Phys. Rept.* **118**, 1 (1985).
 - [66] E. Calzetta and B. L. Hu, *Phys. Rev. D* **37**, 2878 (1988).
 - [67] E. Calzetta and B. L. Hu, *Phys. Rev. D* **35**, 495 (1987).
 - [68] M. Garny and M. M. Miller, *Phys. Rev. D* **80**, 085011 (2009), 0904.3600.
 - [69] S. Borsanyi and U. Reinosa (2008), 0809.0496.
 - [70] V. pika and P. Lipavsk, *Phys. Rev. B* **52**, 14615 (1995).
 - [71] H. S. Khler, *Phys. Rev. C* **46**, 1687 (1992).
 - [72] H. S. Khler and R. Malfiet, *Phys. Rev. C* **48**, 1034 (1993).

- [73] H. S. Khler and K. Morawetz, Phys. Rev. C **64**, 024613 (2001).
- [74] V. G. Morozov and G. Rpke, Cond. mat. Phys. **9**, 473 (2006).
- [75] V. G. Morozov and G. Rpke, Journal of Physics: Conference Series **35**, 110 (2006).
- [76] A. Hohenegger, Phys. Rev. D **79**, 063502 (2009), 0806.3098.